(Preprint) AAS 23-364

OPTIMIZED TRAJECTORY CORRECTION BURN PLACEMENT FOR NRHO ORBIT MAINTENANCE

David Woffinden*, Brayden Barton†

NASA's future Artemis missions plan to utilize a near rectilinear halo orbit (NRHO) in the lunar vicinity to facilitate access to the lunar surface and place other critical assets to support human exploration. This exploration architecture requires a vehicle to remain in the NRHO for long periods of time ranging from several days, to weeks, to months, and even years. Consequently, periodic orbit maintenance burns become essential to ensure the spacecraft follows the desired reference trajectory in an efficient yet effective manner despite crew activity, navigation uncertainty, maneuver execution errors, disturbance accelerations, orbit insertion dispersions, and other system limitations. This work introduces a targeting algorithm that can be utilized to analyze a variety of targeting constraints and parameters that maximizes overall performance. Techniques associated with robust trajectory optimization are used to identify the optimized number and placement for NRHO trajectory correction (NTC) burns that accounts for the mission schedule, both a primary and backup navigation system, targeting strategies and burn plan configurations, vehicle venting, thruster selection, and integrated GN&C performance. A notional scenario extracted from the NASA Artemis III mission is used to motivate and demonstrate these concepts and performance results.

INTRODUCTION

As NASA's exploration initiatives continue to mature, fundamental to its long term objectives is utilizing an Earth-Moon Near Rectilinear Halo Orbit (NRHO) [1, 2] to facilitate access to the lunar surface and enable exploration to Mars and beyond. Not only do plans exist to place a crew-tended lunar Gateway vehicle that has a long term presence in the NRHO as a staging point for both robotic and crewed lunar surface missions, but the Orion spacecraft and other vehicles core to the Human Landing System (HLS) program rely upon the NRHO to support a variety of future Artemis mission objectives. As depicted in Figure 1(a), the NRHO is a subset of the halo orbit families and is characterized by a close passage over one of the lunar poles. The NRHO proposed for future Gateway and Artemis missions is a southern NRHO which reaches the furthest distance from the Moon over the lunar south pole and has a period of approximately seven days.

For upcoming Artemis missions the Orion spacecraft needs to perform strategic orbit maintenance trajectory correction burns to remain near this desired reference profile to support access for lunar landing and return activities as illustrated in Figure 1(b) and Figure 1(c) respectively. Considerable attention has already been made to identify long-term NRHO station-keeping strategies for the Gateway program where techniques have been identified to support orbit maintenance for months and years for a vehicle that is largely unoccupied by crew [3, 4]. Near term Artemis missions have an alternate need for NRHO orbit maintenance such that these NRHO trajectory correction (NTC) burns ensure the Orion spacecraft properly remains near the NRHO to support rendezvous and docking with an HLS lander following its ascent from exploring the lunar surface. In this scenario, both vehicles have extensive crew activity and orbit maintenance is only required for time periods of days or perhaps weeks. As emphasized in Figure 1(c), ensuring Orion is in the proper NRHO location at the proper time when the HLS lander returns back to the NRHO for the NRHO insertion (NRI) burn in preparation for rendezvous, proximity operations, and docking (RPOD) is a critical objective. Given the limited consumables on each mission, a companion objective must be to minimize propellant usage.

*Aerospace Engineer, GN&C Autonomous Flight Systems Branch, NASA Johnson Space Center, Houston TX, 77058
†Graduate student and NASA JSC Intern, Mechanical and Aerospace Engineering, Utah State University, Logan UT, 84322

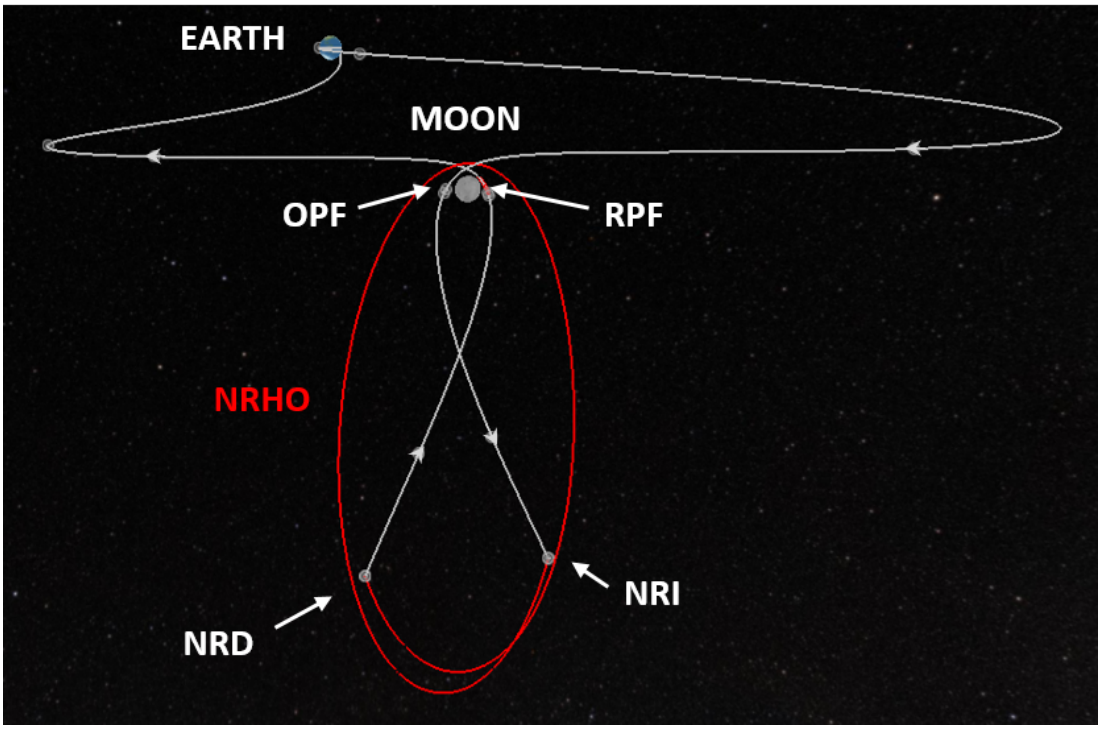

(a) Notional Orion Artemis III Trajectory to a Southern Near Rectilinear Halo Orbit (NRHO).

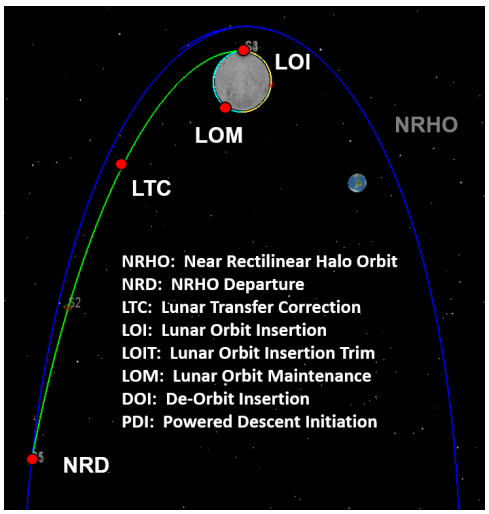

(b) NRHO to LLO Trajectory for HLS Lunar Landing

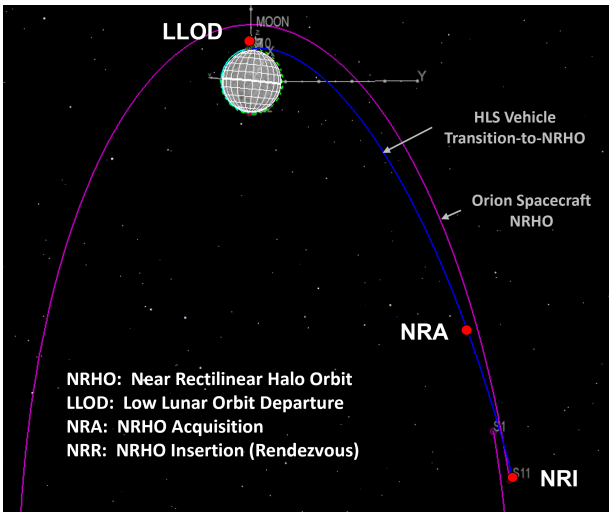

(c) LLO to NRHO Trajectory for HLS Re-Rendezvous

Figure 1. Notional Orion Artemis III Concept of Operations

This paper begins investigating the optimized number and placement of these trajectory correction burns that accounts for uncertainty in the system, the non-linear dynamics of the NRHO trajectory, the geometry of the utilized sensor measurements from the ground tracking stations of the primary navigation system along with the geometry of the Earth and Moon for the backup optical navigation system, the crew schedule on both the Orion and HLS vehicles, spacecraft venting and other disturbance accelerations, targeting and burn plan configurations, thruster selection and actuation errors, and the complex interaction of the overall integrated guidance, navigation, and control (GN&C) system and selected algorithms. Robust trajectory optimization

techniques are adopted to solve this comprehensive problem which utilizes linear covariance (LinCov) analysis [5,6] interfaced with a genetic algorithm (GA). To evaluate an assortment of potential targeting constraints, parameters, and burn plan configurations on the impact of orbit maintenance, a new targeting algorithm is introduced to support rapid analysis need for this type of optimization approach. The ultimate objective is to minimize the total delta-v usage (nominal plus 3-sigma delta-v dispersions) while constraining the Orion trajectory dispersions in the NRHO to remain within the allocated performance specifications to support rendezvous and docking.

The use of these non-traditional robust trajectory optimization or robust trajectory design techniques were originally developed and demonstrated for rendezvous applications in low Earth orbit [7]. It was then extended to cis-lunar outbound trajectories to an NRHO [8] and introduced for a simple rendezvous approach trajectory in the NRHO for mid-course correction placement [9]. Recently, these robust trajectory optimization principles have been applied to solve cislunar transfers to low-lunar orbit [10], NRHO rendezvous and docking [11], lunar powered descent and landing [12], along with Mars aerocapture [13] problems. They are currently being exercised to also determine the optimized trajectory correction burn placement for the upcoming Artemis II free-return cis-lunar trajectory profile [14]. This research applies these same principles to a notional NASA Artemis III scenario where Orion performs orbit maintenance burns in the NRHO while the HLS lunar lander descends to the lunar surface and eventually returns to the NRHO to rendezvous and dock with Orion prior to the HLS crew reentering the Orion spacecraft and departing the NRHO back to Earth.

ANALYSIS APPROACH

Performance Metrics

To optimize the performance of the NRHO orbit maintenance trajectory correction burns to system uncertainty, there are several performance metrics that are utilized which include the true trajectory dispersions $\delta\mathbf{x}$, the navigation dispersions $\delta\hat{\mathbf{x}}$, the true navigation error $\delta\mathrm{e}$, and the onboard navigation error $\delta\hat{\mathrm{e}}$ as depicted in Figure 2. The true dispersions $\delta\mathbf{x}$ are defined as the difference between the true state $\mathbf{x}$ and the nominal state

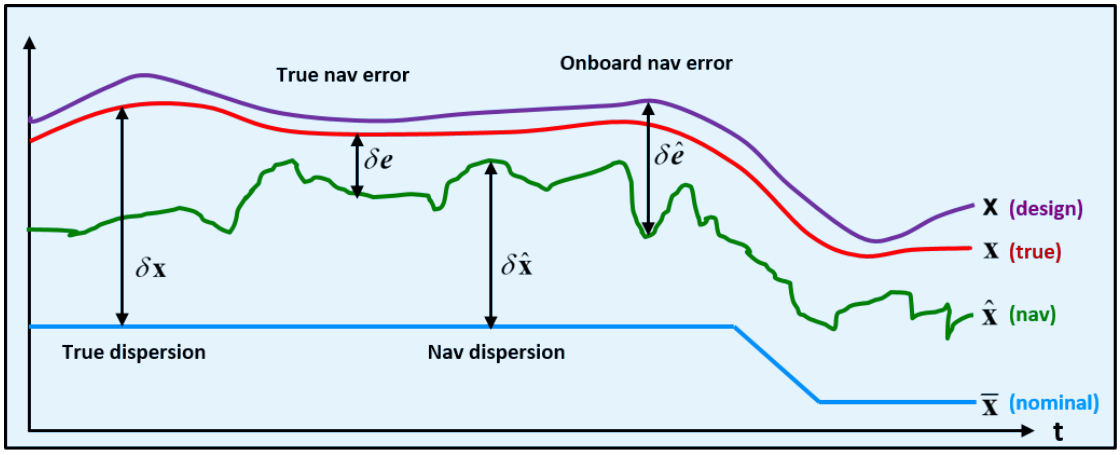

Figure 2. GN&C Performance Metric Variables

$\bar{\mathbf{x}}$. The true state $\mathbf{x}$ is an n-dimensional vector that represents the *real world* environment or actual state.

$$\delta\mathbf{x} \triangleq \mathbf{x} - \bar{\mathbf{x}} \qquad\qquad \mathbf{D} = E\left[\delta\mathbf{x}\delta\mathbf{x}^{\mathrm{T}}\right] \tag{1}$$

The nominal state $\bar{\mathbf{x}}$ is also an n-dimensional vector that represents the desired or reference state. The covariance of the environment dispersions, $\mathbf{D}$, indicates how precisely the system can follow a desired trajectory.

The navigation dispersions $\delta\hat{\mathbf{x}}$ are defined as the difference between the navigation state $\hat{\mathbf{x}}$ and the nominal state $\bar{\mathbf{x}}$. The navigation state is an $\hat{n}$-dimensional vector ($\hat{n} < n$) that represents the filter's estimated state.

$$\delta\hat{\mathbf{x}} \triangleq \hat{\mathbf{x}} - \mathbf{M}_x\bar{\mathbf{x}} \qquad\qquad \hat{\mathbf{D}} = E\left[\delta\hat{\mathbf{x}}\delta\hat{\mathbf{x}}^{\mathrm{T}}\right] \tag{2}$$

The matrix $\mathbf{M}_x$ is an $(\hat{n} \times n)$ matrix that maps the estimated state in terms of the true and nominal state. The covariance of the navigation dispersions, $\hat{\mathbf{D}}$, reflect how precisely the onboard system thinks it can follow a prescribed reference trajectory.

The true navigation error $\delta\mathbf{e}$ is the difference between the environment and navigation states. It is also the difference between the environment and the navigation dispersions.

$$\delta\mathbf{e} \triangleq \mathbf{M}_x\mathbf{x} - \hat{\mathbf{x}} = \mathbf{M}_x\delta\mathbf{x} - \delta\hat{\mathbf{x}} \qquad\qquad \mathbf{P} = E\left[\delta\mathbf{e}\delta\mathbf{e}^{\mathrm{T}}\right] \tag{3}$$

The covariance of the true navigation error, $\mathbf{P}$, quantifies how precisely the onboard navigation system can estimate the actual state.

The onboard navigation error $\delta\hat{\mathbf{e}}$ itself is never computed, but it is used to develop the onboard navigation filter equations. It is defined as the difference between the design state, x, and the navigation state $\hat{\mathbf{x}}$.

$$\delta\hat{\mathbf{e}} \triangleq \mathrm{x} - \hat{\mathbf{x}} \qquad\qquad \hat{\mathbf{P}} = E\left[\delta\hat{\mathbf{e}}\delta\hat{\mathbf{e}}^{\mathrm{T}}\right] \tag{4}$$

The covariance of the onboard navigation error, $\hat{\mathbf{P}}$, quantifies how precisely the onboard navigation system expects it can determine the actual state. The performance of the onboard navigation system is determined by comparing $\hat{\mathbf{P}}$ to the actual navigation performance $\mathbf{P}$. If the *true* states and the *design* states are assumed to be the same, then the true navigation covariance will equal the onboard navigation covariance.

The covariances of the true dispersions, navigation dispersions, true navigation error, and the onboard navigation error are ultimately used to analyze and assess the performance of a proposed GN&C system. A common approach to obtain these performance metrics is to use a Monte Carlo simulation outlined in Figure 3, where the sample statistics of hundreds or thousands of runs, N, are used to numerically compute the desired covariance matrices.

$$\mathbf{D} = \frac{1}{N-1}\sum \delta\mathbf{x}\delta\mathbf{x}^{\mathrm{T}} \qquad \hat{\mathbf{D}} = \frac{1}{N-1}\sum \delta\hat{\mathbf{x}}\delta\hat{\mathbf{x}}^{\mathrm{T}} \qquad \mathbf{P} = \frac{1}{N-1}\sum \delta\mathbf{e}\delta\mathbf{e}^{\mathrm{T}} \tag{5}$$

The onboard navigation error covariance $\hat{\mathbf{P}}$ is the navigation filter covariance for each run. This same statistical information can be obtained using linear covariance analysis techniques.

Linear covariance analysis incorporates the non-linear system dynamics models and GN&C algorithms to generate a nominal reference trajectory $\bar{\mathbf{x}}$ which is then used to propagate, update, and correct an onboard navigation covariance matrix $\hat{\mathbf{P}}$ and an augmented state covariance matrix $\mathbf{C}$,

$$\mathbf{C} = E\left[\delta\mathbf{X}\delta\mathbf{X}^{\mathrm{T}}\right] \tag{6}$$

where the augmented state $\delta\mathbf{X}^{\mathrm{T}} = [\delta\mathbf{x}^{\mathrm{T}}\ \delta\hat{\mathbf{x}}^{\mathrm{T}}]$ consists of the true dispersions and the navigation dispersions. Pre- and post-multiplying the augmented state covariance matrix by the following mapping matrices, the covariances for the trajectory dispersions, navigation dispersions, and the navigation error can be obtained.

$$\begin{aligned}
\mathbf{D} &= [\,\mathbf{I}_{n\times n},\ \mathbf{0}_{n\times\hat{n}}\,]\,\mathbf{C}\,[\,\mathbf{I}_{n\times n},\ \mathbf{0}_{n\times\hat{n}}\,]^{\mathrm{T}} \\
\hat{\mathbf{D}} &= [\,\mathbf{0}_{\hat{n}\times n},\ \mathbf{I}_{\hat{n}\times\hat{n}}\,]\,\mathbf{C}\,[\,\mathbf{0}_{\hat{n}\times n},\ \mathbf{I}_{\hat{n}\times\hat{n}}\,]^{\mathrm{T}} \\
\mathbf{P} &= [\,\mathbf{I}_{\hat{n}\times n},\ -\mathbf{I}_{\hat{n}\times\hat{n}}\,]\,\mathbf{C}\,[\,\mathbf{I}_{\hat{n}\times n},\ -\mathbf{I}_{\hat{n}\times\hat{n}}\,]^{\mathrm{T}}
\end{aligned} \tag{7}$$

Linear Covariance Analysis

The linear covariance analysis equations used to propagate, update, and correct both the augmented state covariance matrix and the onboard navigation covariance matrix are summarized here along with the LinCov analysis inputs. For additional details regarding the development and implementation of the linear covariance simulation, see the following references [5, 6, 15–18].

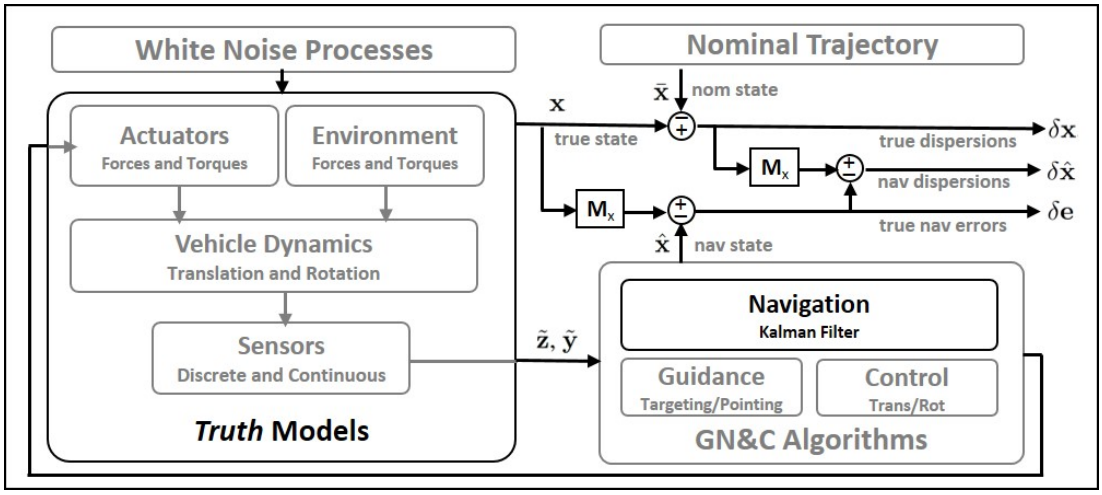

Figure 3. Extracting GN&C Performance Metrics Using Monte Carlo Techniques

Propagate The discrete-time propagation equations for augmented state covariance matrix $\mathbf{C}$ and the onboard navigation covariance matrix $\hat{\mathbf{P}}$ are

$$\mathbf{C}(t_{k+1}) = \mathbf{\Phi}(t_{k+1}, t_k)\mathbf{C}(t_k)\mathbf{\Phi}^T(t_{k+1}, t_k) + \mathbf{G}\mathbf{Q}\mathbf{G}^T \tag{8}$$

$$\hat{\mathbf{P}}(t_{k+1}) = \hat{\mathbf{\Phi}}(t_{k+1}, t_k)\hat{\mathbf{P}}(t_k)\hat{\mathbf{\Phi}}^T(t_{k+1}, t_k) + \hat{\mathbf{G}}\hat{\mathbf{Q}}\hat{\mathbf{G}}^T \tag{9}$$

where $\mathbf{\Phi}$ and $\hat{\mathbf{\Phi}}$ are augmented and onboard state transition matrices respectively for the linearized perturbation dynamics about the reference trajectory. The mapping matrices, $\mathbf{G}$ and $\hat{\mathbf{G}}$, are used to map environmental and navigation process noise characterized by $\mathbf{Q}$ and $\hat{\mathbf{Q}}$, into $\mathbf{C}$ and $\hat{\mathbf{P}}$.

Update The measurement update equations for augmented and navigation state covariance matrices, $\mathbf{C}$ and $\hat{\mathbf{P}}$, at a measurement time t_i are

$$\mathbf{C}^+(t_i) = \mathbf{A}\mathbf{C}^-(t_i)\mathbf{A}^T + \mathbf{B}\mathbf{R}^j(t_i)\mathbf{B}^T \tag{10}$$

$$\hat{\mathbf{P}}^+(t_i) = \left[\hat{\mathbf{I}} - \hat{\mathbf{K}}^j(t_i)\hat{\mathbf{H}}^j\right]\hat{\mathbf{P}}^-(t_i)\left[I - \hat{\mathbf{K}}^j(t_i)\hat{\mathbf{H}}^j\right]^T + \hat{\mathbf{K}}^j(t_i)\hat{\mathbf{R}}^j(t_i)\hat{\mathbf{K}}^j(t_i)^T \tag{11}$$

where the superscript 'j' denotes the jth measurement type. The Kalman gain is written as

$$\hat{\mathbf{K}}^j(t_i) = \hat{\mathbf{P}}(t_i)(\hat{\mathbf{H}}^j)^T\left[\hat{\mathbf{H}}^j\hat{\mathbf{P}}^-(t_i)(\hat{\mathbf{H}}^j)^T + \hat{\mathbf{R}}^j(t_i)\right]^{-1} \tag{12}$$

The matrices $\hat{\mathbf{H}}$ and $\hat{\mathbf{R}}$ are the measurement sensitivity and measurement noise matrices respectively. The matrices $\mathbf{A}$ are $\mathbf{B}$ map the effects of the measurements and their associated noise to the navigation state dispersions.

Correct The correction equations for impulsive translational burns for the augmented state and onboard state covariances, $\mathbf{C}$ and $\hat{\mathbf{P}}$, at a maneuver time t_m are

$$\mathbf{C}^+(t_m) = \mathbf{M}\mathbf{C}^-(t_m)\mathbf{M}^T + \mathbf{N}\boldsymbol{Q}_w^{act}\mathbf{N}^T \tag{13}$$

$$\hat{\mathbf{P}}^+(t_m) = \left[\hat{\mathbf{I}} + \hat{\mathbf{M}}\right]\hat{\mathbf{P}}^-(t_m)\left[I + \hat{\mathbf{M}}\right]^T + \hat{\mathbf{N}}\hat{\mathbf{Q}}_w^{act}\hat{\mathbf{N}}^T \tag{14}$$

The matrices $\mathbf{M}$ and $\hat{\mathbf{M}}$ contain the control partials associated with a linearized two-impulse targeting algorithm. The matrices $\mathbf{N}$ and $\hat{\mathbf{N}}$ are used to map the effects of actuator noise, described by $\boldsymbol{Q}_w^{act}$ and $\hat{\mathbf{Q}}_w^{act}$, into $\mathbf{C}$ and $\hat{\mathbf{P}}$.

Optimization Problem Formulation

The optimization problem formulation for this analysis utilizes several key metrics [19]; the standard deviations of the delta-v dispersions $\sigma_{\delta\Delta v}$, position dispersions $\sigma_{\delta r}$, and velocity dispersions $\sigma_{\delta v}$. These quantities are extracted from the dispersion covariance, $\mathbf{C}$. Depending on the mission objectives and priorities, the optimization problem can be specified several different ways. For this study, three different problem formulations are evaluated which are defined below as Problem #1, Problem #2, and Problem #3. Each of their corresponding objective functions incorporate several constraints to ensure the vehicle does not exceed the following limits to support subsequent RPOD activities: a 20 km NRHO insertion (NRI) maximum position dispersion $3\sigma_{\delta r}^{req}$, a 1 m/s post-NRI maximum velocity dispersion $3\sigma_{\delta v}^{req}$, and a total NRHO orbit maintenance delta-v (nominal + 3-sigma dispersions) $3\sigma_{\Delta v}^{req}$ of 20 m/s.

$$3\sigma_{\delta r}^{req} = 20 \text{ km} \tag{15}$$
$$3\sigma_{\delta v}^{req} = 1 \text{ m/s} \tag{16}$$
$$3\sigma_{\Delta v}^{req} = 20 \text{ m/s} \tag{17}$$

Other underlying constraints imposed in the optimization process is that the earliest a trajectory correction burn can occur is one hour after the HLS vehicle NRHO departure (NRD). The last NTC burn must be one hour prior to HLS's NRHO insertion (NRI). Also, each NTC burn must be separated from another by at least one hour. The timing for the NRD burn and the NRI burns are fixed.

Problem #1 The first objective function, minimizes the total delta-v Δv_{total} which consists of the nominal plus 3-sigma delta-v dispersions across all NTC burns subject to a constraint on the position and velocity dispersions at the NRHO insertion (NRI) location. For Problem #1, the NRI position dispersion and velocity constraints are implemented as a penalty function. When a constraint is violated, a large penalty κ is added to the objective function,

$$\text{minimize} \quad (\Delta v_{total} + \kappa_{\delta r} + \kappa_{\delta v} + \kappa_{ntc}) \tag{18}$$

where the penalty for violating the constraint for the NRI position dispersions $\kappa_{\delta r}$, the NRI velocity dispersions κ_{δ}, and an operational penalty for performing each trajectory correction burn κ_{ntc} (if applied) are specified as,

$$\Delta v_{total} = \sum_{m=1}^{N} \left[\Delta\bar{v}(t_m) + 3\sigma_{\Delta v}(t_m)\right]$$

$$\kappa_{\delta r} = \begin{cases} \left(1 \times 10^6\right) + \left(3\sigma_{\Delta v}^{req}\left[\sigma_{\delta r}(t_{nri})/\sigma_{\delta r}^{req}\right]\right), & \text{if } \sigma_{\delta r}(t_{nri}) > \sigma_{\delta r}^{req} \\ 0, & \text{otherwise} \end{cases}$$

$$\kappa_{\delta v} = \begin{cases} \left(1 \times 10^6\right) + \left(3\sigma_{\Delta v}^{req}\left[\sigma_{\delta v}(t_{nri})/\sigma_{\delta v}^{req}\right]\right), & \text{if } \sigma_{\delta v}(t_{nri}) > \sigma_{\delta v}^{req} \\ 0, & \text{otherwise} \end{cases}$$

$$\kappa_{ntc} = \begin{cases} n_{tc} * \left(3\sigma_{\Delta v}^{req}/20\right), & \text{if activated, adds 1 m/s penalty for each burn} \\ 0, & \text{otherwise} \end{cases}$$

Problem #2 The second objective function, minimizes the 3-sigma position dispersions at NRI subject to constraints on the total delta-v (nominal plus 3-sigma delta-v dispersions) and the NRI velocity dispersions. The total delta-v and NRI velocity dispersion constraints are implemented as penalties to the cost function below,

$$\text{minimize} \quad (\ 3\sigma_{\delta r}(t_{nri}) + \kappa_{\Delta v} + \kappa_{\delta v} + \kappa_{ntc}\ ) \tag{19}$$

where the penalty for violating the constraint for the total delta-v $\kappa_{\Delta v}$, the NRI velocity dispersions κ_{δ}, and an operational penalty for performing each trajectory correction burn κ_{ntc} (if applied) are specified as,

$$\begin{aligned}
\Delta v_{total} &= \sum_{m=1}^{N} \left[\Delta\bar{v}(t_m) + 3\sigma_{\Delta v}(t_m)\right] \\
\kappa_{\Delta v} &= \begin{cases} \left(1\times10^6\right) + \left(3\sigma_{\delta r}^{req}\left[\Delta v_{total}/\sigma_{\Delta v}^{req}\right]\right), & \text{if } \Delta v_{total} > 3\sigma_{\Delta v}^{req} \\ 0, & \text{otherwise} \end{cases} \\
\kappa_{\delta v} &= \begin{cases} \left(1\times10^6\right) + \left(3\sigma_{\delta r}^{req}\left[\sigma_{\delta v}(t_{nri})/\sigma_{\delta v}^{req}\right]\right), & \text{if } \sigma_{\delta v}(t_{nri}) > \sigma_{\delta v}^{req} \\ 0, & \text{otherwise} \end{cases} \\
\kappa_{ntc} &= \begin{cases} n_{tc} * \left(3\sigma_{\delta r}^{req}/40\right), & \text{if activated, adds 0.5 km penalty for each burn} \\ 0, & \text{otherwise} \end{cases}
\end{aligned}$$

Problem #3 The third objective function, simultaneously minimizes both the total delta-v and the 3-sigma position dispersions at NRI subject to constraints on the NRI velocity dispersions and the total numbers of burns (if applied). The NRI velocity dispersion constraint is implemented as a penalty to the cost function below,

$$\text{minimize} \quad \left(w_{\Delta v} * \Delta v_{total} + w_{\delta r} * 3\sigma_{\delta r}(t_{nri}) + \kappa_{\delta v} + \kappa_{ntc}\right) \tag{20}$$

where the penalty for violating the constraint for the total delta-v $\kappa_{\Delta v}$, the NRI velocity dispersions κ_{δ}, and an operational penalty for performing each trajectory correction burn κ_{ntc} (if applied) are specified as,

$$\begin{aligned}
\Delta v_{total} &= \sum_{m=1}^{N} \left[\Delta\bar{v}(t_m) + 3\sigma_{\Delta v}(t_m)\right] \\
\kappa_{\delta v} &= \begin{cases} \left(1\times10^6\right) + \left(3\sigma_{\delta r}^{req}\left[\sigma_{\delta v}(t_{nri})/\sigma_{\delta v}^{req}\right]\right), & \text{if } \sigma_{\delta v}(t_{nri}) > \sigma_{\delta v}^{req} \\ 0, & \text{otherwise} \end{cases} \\
\kappa_{ntc} &= \begin{cases} n_{tc} * \left(3\sigma_{\delta r}^{req}/40\right), & \text{if activated} \\ 0, & \text{otherwise} \end{cases} \\
w_{\Delta v} &= 100 * w/\sigma_{\Delta v}^{req} \text{ , where } w = 0.5 \\
w_{\delta r} &= 100 * (1-w)/\sigma_{\delta r}^{req}
\end{aligned}$$

LinCov Embedded in a Genetic Optimization Algorithm

Due to their complex nature, the optimization problem is solved using a genetic algorithm (GA). A genetic algorithm is a type of optimization solver which employs evolutionary processes to search a solution space [20]. A population of candidates is generated, evaluated, and based on their performance a new generation is created by combining and mutating them. During each iteration, candidate values of the optimization variables are passed to the LinCov simulation, which is then evaluated to determine the values of the cost and penalty functions. This process is shown in Figure 4.

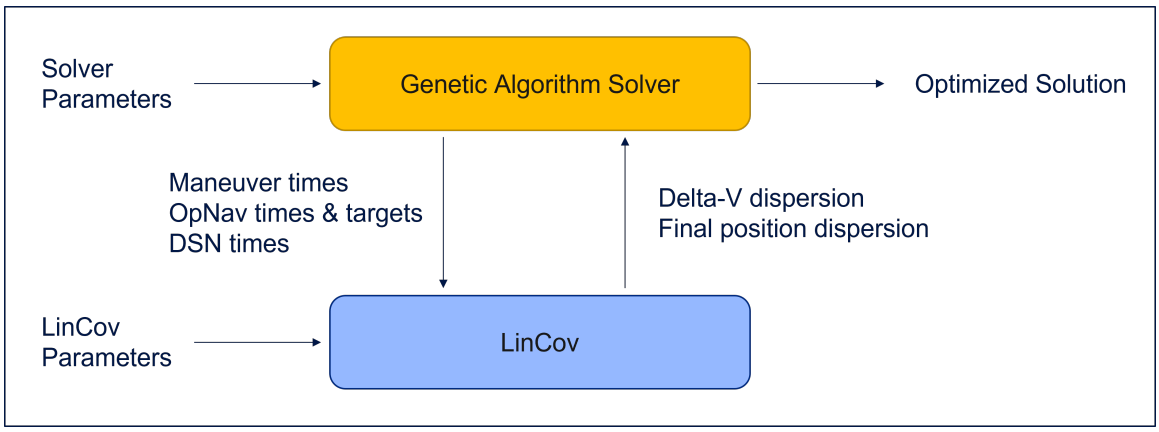

Figure 4. Functional relationship between the LinCov simulation and Genetic Algorithm.

For each of the optimization runs performed using the genetic algorithm, a population size of 30 was selected along with a maximum generation of 30. Both a larger population size and maximum number of generations are preferable, but due to run time limitations, the selected values provided a reasonable compromise between solution accuracy and speed to identify top level trends.

GN&C MODELING

Excluding the uncertainty in the trajectory design process, the magnitude of the NRHO orbit maintenance burns, regardless of where they are placed, are nominally zero. Consequently, the optimization of the number and location of the trajectory correction burns is driven by the implementation of the vehicle's GN&C system in context of the baseline NRHO reference trajectory, the operational time line, navigation modes, target configurations and burn plans, along with venting and disturbance acceleration modeling. This section contains the GN&C modeling assumptions and parameter specification that influences the optimized burn placement.

Nominal NRHO Trajectory Profile and Concept of Operations

Details related to a notional Artemis III NRHO orbit maintenance scenario along with flight operation activities prior, during, and following this phase are provided in Figure 5. The illustration in Figure 5(a) captures the complex sequence of events following Orion's insertion in the NRHO indicated with a red dot on the dashed yellow line labeled *1st Dock*, to the HLS lander departure from the NRHO (NRD) shown with the solid yellow line, to the return of the HLS lander from the lunar surface to the NRHO for *2nd Dock* highlighted with a solid green line, to post docking and preparations for Orion to depart the NRHO to return back to Earth depicted with a solid light blue line.

The key segment for this study is the phase immediately after the HLS lander departs for the lunar surface while Orion remains in the NRHO. It is assumed just prior to the HLS NRD burn, both vehicles have contact with the ground, received an authority to proceed, and have a current uplinked state estimate of both vehicles along with an updated burn plan based on the current NRHO reference trajectory the two vehicles are following. If for any reason the two vehicles are unable to communicate with each other or the ground, the designated re-rendezvous point for the second docking would be the assumed location for the HLS NRHO insertion. Orion would need to ensure it performs sufficient NRHO orbit maintenance burns such that the two vehicles can acquire one another with the designated relative navigation sensors to support subsequent RPOD operations.

The plot provided in Figure 5(b) gives context to how a vehicle transfers along the NRHO orbit and the corresponding distances from the moon. The yellow dots indicate the location of a vehicle at half-day increments starting from perilune. Rather than reporting the specific times of each optimized trajectory correction

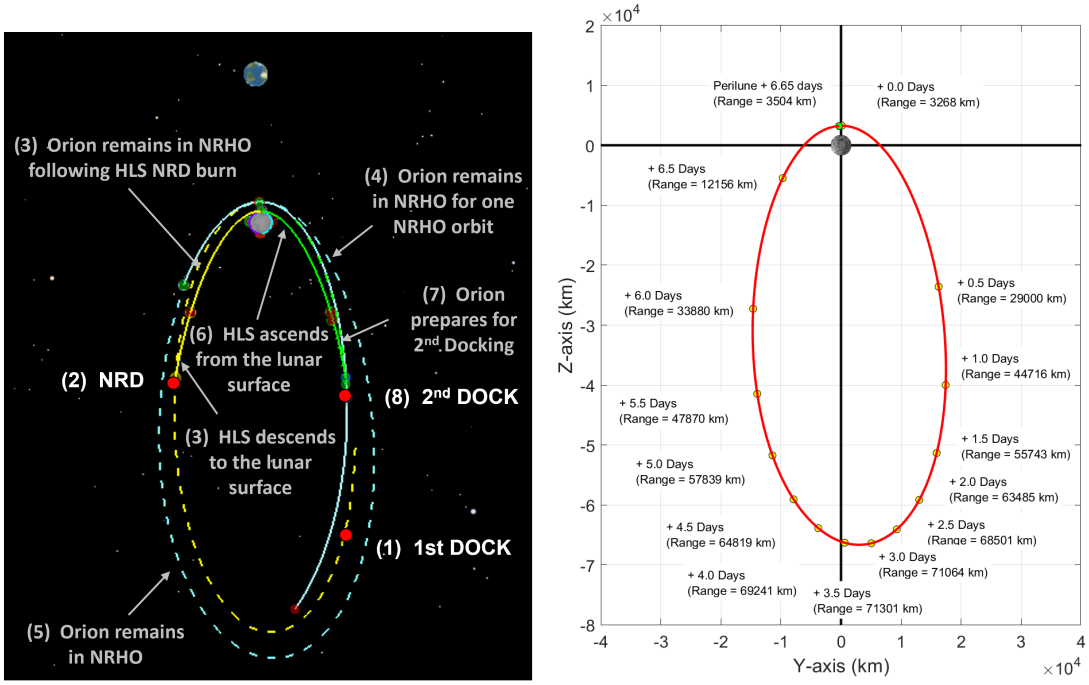

(a) Notional Artemis III NRHO trajectory overview.

(b) NRHO Timing and Lunar Distances

Figure 5. Notional Orion Artemis III NRHO Orbit Maintenance Concept of Operations

burn placement, they will be provided graphically and this figure can provide intuition as to the time interval between correction burns.

To highlight the impacts of optimizing the NTC burn placement to support NRHO orbit maintenance, a notional baseline is specified where the NTC burns are placed at one-day increments. This notional strategy would have the crew consistently execute an NTC burn scheduled near the same time each day. Under this premise, there will be seven NTC burns with the last one placed 6 hours prior to NRI. The major events, scheduling, targeting strategies, and sensor utilization for the baseline NRHO orbit maintenance scenario is provided in Table 1. Baseline performance values are provided for having 7 NTCs (NTC1, NTC2, NTC3, NTC4, NTC5, NTC6, and NTC7), 4 NTCs (NTC1, NTC3, NTC5, and NTC7), and 2 NTCs (NTC3 and NTC7). These baseline burn plans are then optimized by shifting the corresponding trajectory correction burn times.

The scenario starts one hour prior to the HLS NRHO departure (NRD) burn. A DSN ground tracking pass update is uplinked to both vehicles 15 minutes prior to NRD. If the lander has significant dispersions prior to NRD due to limited NRHO orbit maintenance burns while a stacked configuration, the ground will also upload a new NRHO reference trajectory or burn plan. The Orion NRD burn is executed using a two-level targeter (TLT) that targets the NRHO insertion (NRI) point 7 days, 11 hours, and 24 minutes into the future. It corrects for any undocking and departure induced accelerations and displacements. This initial NRD burn is supported using the DSN ground update, accelerometer, gyros, and a star tracker. In general, prior to each burn and afterwards, either a DSN ground estimate is uplinked to the spacecraft to support targeting and burn execution or an optical navigation (OpNav) pass is performed. The subsequent NTC burns are performed with *kernel targeting* to accelerate the optimization process while capturing the effects of targeting the NRI position. At NRI, Orion performs a burn to ensure its velocity matches the nominal NRHO referent trajectory velocity. This ensures Orion is closely aligned with the predetermined NRHO reference trajectory and phase. The simulation epoch is *2025 Jan 31 17:57:50.82* (or ET *791618340.004785* sec).

Table 1. Baseline NRHO Orbit Maintenance Concept of Operations

Event	Description	MET	Targeting	Sensors
START	NRHO Orbit Starting Point	0:00:00:00		IMU, Startracker, DSN
NRD	NRHO Departure Burn	0:01:00:00	TLT (Pos)	IMU, Startracker, DSN*
NTC1	NRHO Correction Burn #1	2:00:00:00	Kernel (Pos)	IMU, Startracker, DSN (or OPNAV)
NTC2	NRHO Correction Burn #2	3:00:00:00	Kernel (Pos)	IMU, Startracker, DSN (or OPNAV)
NTC3	NRHO Correction Burn #3	4:00:00:00	Kernel (Pos)	IMU, Startracker, DSN (or OPNAV)
NTC4	NRHO Correction Burn #4	5:00:00:00	Kernel (Pos)	IMU, Startracker, DSN (or OPNAV)
NTC5	NRHO Correction Burn #5	6:00:00:00	Kernel (Pos)	IMU, Startracker, DSN (or OPNAV)
NTC6	NRHO Correction Burn #6	7:00:00:00	Kernel (Pos)	IMU, Startracker, DSN (or OPNAV)
NTC7	NRHO Correction Burn #7	7:06:24:00	Kernel (Pos)	IMU, Startracker, DSN (or OPNAV)
NRI	NRHO Insertion Burn	7:12:24:00	Kernel (Vel)	IMU, Startracker, DSN (or OPNAV)

Navigation System Modeling

Three different navigation systems are modeled for the trajectory correction burn placement analysis. The first represents a primary navigation system consisting of DSN ground updates, accelerometers, gyros, and star trackers. The second reflects a backup navigation system with an onboard optical navigation (OpNav) system along with accelerometers, gyros, and a star tracker. Lastly, to remove the impacts of the navigation errors on the trajectory correction burn placement analysis, a third navigation system is modeled referred to as *perfect nav*. For this navigation mode, the navigation errors are set to zero such that the navigation estimate equals the truth state. The mathematical models used for the different measurement types are provided below.

DSN Ground Update The Deep Space Network (DSN) ground update provides a position and velocity state estimate and covariance to the lander at designated epochs based on range $\tilde{\rho}$ and doppler measurements $\tilde{\dot{\rho}}$ between the ground tracking station and the spacecraft [21] which are functions of the landers inertial position $\mathbf{r}_l^i$, the lander's mounted antenna location $\mathbf{r}_a^b$, lander's inertial-to-body transformation matrix $\mathbf{T}_b^i$, the lander's angular rate $\boldsymbol{\omega}_l^b$, the inertial-to-planet transformation $\mathbf{T}_p^i$, the Earth's angular rate $\boldsymbol{\omega}_e^p$, the ground station location $\mathbf{r}_{gs}^p$ in the planet-fixed frame, the range bias $\boldsymbol{b}_\rho$, doppler bias $\boldsymbol{b}_{\dot{\rho}}$, range noise $\boldsymbol{\upsilon}_\rho$, and doppler noise $\boldsymbol{\upsilon}_{\dot{\rho}}$.

$$\tilde{\rho} = \left|\mathbf{r}_l^i + \mathbf{T}_b^i \mathbf{r}_a^b - \mathbf{T}_p^i \mathbf{r}_{gs}^p\right| + \boldsymbol{b}_\rho + \boldsymbol{\upsilon}_\rho \tag{21}$$

$$\tilde{\dot{\rho}} = \frac{\left[\mathbf{v}_l^i + \mathbf{T}_b^i\left(\boldsymbol{\omega}_l^b \times \mathbf{r}_a^b\right) - \mathbf{T}_p^i\left(\boldsymbol{\omega}_e^p \times \mathbf{r}_{gs}^p\right)\right]^{\mathrm{T}}\left[\mathbf{r}_l^i + \mathbf{T}_b^i \mathbf{r}_a^b - \mathbf{T}_p^i \mathbf{r}_{gs}^p\right]}{\left[\mathbf{r}^i + \mathbf{T}_b^i \mathbf{r}_a^b - \mathbf{T}_p^i \mathbf{r}_{gs}^p\right]} + \boldsymbol{b}_{\dot{\rho}} + \boldsymbol{\upsilon}_{\dot{\rho}} \tag{22}$$

The uncertainty parameters used for the DSN ground updates are given in Table 2.

OpNav The optical navigation (OpNav) system produces bearing measurements to the centroid of a celestial body, both a horizontal α_h and vertical α_v, along with a range measurement ρ based on the apparent angular diameter of the planet. OpNav measurements are functions of the centroid and apparent angular biases b, noise η, and pointing error. Rather than processing the *raw* angles, the tangent of the angles are utilized, $\tilde{y}_h$ and $\tilde{y}_v$ [22]. Conceptually, the core measurements are

$$\tilde{y}_h = \tan(\alpha_h) + b_h + \eta_h = x/z + b_h + \eta_h \tag{23}$$

$$\tilde{y}_v = \tan(\alpha_v) + b_v + \eta_v = y/z + b_v + \eta_v \tag{24}$$

$$\tilde{\rho} = \rho + b_\rho + \eta_\rho = \sqrt{x^2 + y^2 + z^2} + b_\rho + \eta_\rho \tag{25}$$

where $\boldsymbol{\rho}^T = (\mathbf{r}_o - \mathbf{r}_p)^T = [x, y, z]$ and the *range* measurement $\tilde{\rho}$ is actually converted to an apparent angular diameter and all the measurements are processed in terms of pixels. The parameters used for the OpNav

system are provided in Table 6. The uncertainty of OpNav measurements depend on the celestial body, range to celestial body, and camera specifications.

The OpNav field of view (FOV) constraint shown in Table 6 is dependent on camera properties and equal to 20 degrees. If the apparent angular diameter of the target celestial body exceeds the FOV constraint, no OpNav measurements are taken. Lighting constraints were not activated for this study. Lastly, to ensure that navigation never goes more then a day without a lunar OpNav measurement, an Opnav pass is always inserted between two burns when they are separated by more than a day.

Accelerometer The accelerometer measures the non-gravitational acceleration in the IMU case frame $\tilde{\mathbf{a}}^{imu}$, which is a function of the nominal inertial-to-body transformation matrix $\bar{\mathbf{T}}_i^b$, the nominal body-to-IMU transformation $\bar{\mathbf{T}}_b^{imu}$, the actual attitude dispersion $\boldsymbol{\theta}$, the misalignment $\boldsymbol{\mu}_a$, the constant scale factor $\mathbf{s}_a$, the Markov scale factor $\boldsymbol{\sigma}_a$, the constant bias $\mathbf{b}_a$, the Markov bias $\boldsymbol{\beta}_a$, the nonorthogonality factor $\boldsymbol{\gamma}_a$, and the velocity random walk (noise) $\boldsymbol{\upsilon}_a$.

$$\tilde{\mathbf{a}}^{imu} = (\mathbf{I} + [(\mathbf{s}_a + \boldsymbol{\sigma}_a)\diagdown]) \left[(\mathbf{I} + [\boldsymbol{\mu}_a\times]) (\mathbf{I} + [\boldsymbol{\gamma}_a *]) \bar{\mathbf{T}}_b^{imu} (\mathbf{I} + [\boldsymbol{\theta}\times]) \bar{\mathbf{T}}_i^b \mathbf{a}^i + \mathbf{b}_a + \boldsymbol{\beta}_a + \boldsymbol{\upsilon}_a\right] \tag{26}$$

The uncertainty parameters used for the accelerometer are listed in Table 3.

Gyro The gyros measure the vehicle's angular rates in the IMU case frame $\tilde{\boldsymbol{\omega}}^{imu}$ and is represented as a function of the nominal body-to-IMU transformation $\bar{\mathbf{T}}_b^{imu}$ where b indicates the vehicle body-fixed frame, the misalignment $\boldsymbol{\mu}_\omega$, the constant scale factor $\mathbf{s}_\omega$, the Markov scale factor $\boldsymbol{\sigma}_\omega$, the constant bias $\mathbf{b}_\omega$, the Markov bias $\boldsymbol{\beta}_\omega$, the nonorthogonality factor $\boldsymbol{\gamma}_\omega$, and the angular random walk (noise) $\boldsymbol{\upsilon}_\omega$

$$\tilde{\boldsymbol{\omega}}^{imu} = (\mathbf{I} + [(\mathbf{s}_\omega + \boldsymbol{\sigma}_\omega)\diagdown]) \left[(\mathbf{I} + [\boldsymbol{\mu}_\omega\times]) (\mathbf{I} + [\boldsymbol{\gamma}_\omega *]) \bar{\mathbf{T}}_b^{imu} \boldsymbol{\omega}^b + \mathbf{b}_\omega + \boldsymbol{\beta}_\omega + \boldsymbol{\upsilon}_\omega\right] \tag{27}$$

The uncertainty parameters used for the gyroscope are listed in Table 4.

Star Tracker The star tracker provides an accurate measurement of the vehicle's orientation. The generated inertial-to-star tracker quaternion is a function of the body-to-star tracker mounting $\mathbf{q}_b^{st}$, the actual inertial-to-body quaternion $\mathbf{q}_i^b$, the sensor bias $\mathbf{b}_{st}$, noise $\boldsymbol{\eta}_{st}$, and misalignment $\boldsymbol{\mu}_{st}$

$$\tilde{\mathbf{q}}_{st}^i = \mathbf{q}(\boldsymbol{\eta}_{st}) \otimes \mathbf{q}(\mathbf{b}_{st}) \otimes \mathbf{q}(\boldsymbol{\eta}_{st}) \otimes \mathbf{q}_b^{st} \otimes \mathbf{q}_i^b \tag{28}$$

The star tracker parameters are summarized in Table 5.

Table 2. DSN Update

Parameter	3σ
Range Noise, m	25
Range-rate Noise, cm/s	1.5
Range Bias, m	25
Range-rate Bias, cm/s	1.5
Elevation Mask, deg	10.0
Max Pass Duration, hr	2.0

Table 3. Accelerometer [23]

Parameter	3σ
VRW, mm/s/sqrt(s)	0.3
Bias, μg	84
Scale Factor, ppm	450
Nonorthogonality, arcsec	17
Markov Bias, μg	84
Markov Scale Factor, ppm	450

Table 4. Gyros [23]

Parameter	3σ
ARW, deg/$\sqrt{hr}$	0.015
Bias, deg/hr	0.036
Scale Factor, ppm	27
Nonorthogonality, arcsec	19
Markov Bias, deg/hr	0.036
Markov Scale Factor, ppm	27

Table 5. Startracker [23]

Parameter	3σ
Boresight Noise, arcsec	72
Crs-Boresight Bias, arcsec	24
Misalignment, deg	0.5

Table 6. OpNav

Parameter	3σ
Celestial Body	Moon
Pass Duration, hr	2
FOV, deg	20

Table 7. Process Noise

Parameter	3σ
Orbit Trans, m/s/$\sqrt{s}$	$0.42e^{-3}$
RPOD Trans, m/s/$\sqrt{s}$	$0.42e^{-3}$
Rotational, rad/s/$\sqrt{s}$	$0.0e^{-6}$

Table 8. Initial Dispersions

Parameter	3σ
Position, km	2
Velocity, cm/s	20
Attitude, deg	0.5
Attitude-Rate, deg/s	0.01

Table 9. Initial Navigation

Parameter	3σ
Position, km	2.0
Velocity, cm/s	2.0
Attitude, deg	0.05
Attitude-Rate, deg/s	0.01

Table 10. Thrusters

Parameter	3σ
Bias, cm/s	8
Noise, cm/s	8
Scale Factor, ppm	7000
Misalignment, deg	0.1

Targeting Algorithms and Models

There are two targeting algorithms used for the NRHO orbit maintenance analysis which includes a two-level targeter (TLT) and kernel targeting. Each computes an impulsive velocity change to help follow a prescribed NRHO reference trajectory. The accuracy of executing the corresponding impulsive burns is also provided.

Two-Level Targeter Following the separation of the target vehicle and after its NRHO departure burn (NRD), Orion notionally performs a clean up burn with an impulsive constrained two-level targeter (TLT) that uses a two-level corrections process to target the desired NRHO insertion (NRI) state [24–28] designated as the point for re-rendezvous. The algorithm works by dividing the trajectory into segments or a series of intermediate targets known as patch states. The first stage, or the level-I process, introduces impulsive maneuvers at the interior patch states until position continuity across all segments is achieved. The second stage, or the level-II process, adjusts the shape of the trajectory by spatially and temporally relocating the patch states to drive the velocity discontinuities to zero. This approach is not limited to merely targeting a terminal position vector, but any terminal constraint such as flight path angle, altitude, velocity magnitude, or any function of the position and velocity state.

Kernel Targeting The subsequent trajectory correction burns aim to keep the Orion spacecraft along the specified NRHO reference trajectory with the proper phase angle. Nominally, these burns have a delta-v magnitude of zero. The following strategy is adopted that utilizes a kernel, or the actual time history data of the reference trajectory, to compute the necessary delta-v in a fast and efficient manner. As the name alludes to, kernel targeting relies on a trajectory kernel, typically associated with the Navigation and Ancillary Information Facility (NAIF) information system *SPICE* kernel or SPK-file. The letter 'S' in SPICE refers to the *Spacecraft ephemeris, given as a function of time* while the letter 'P' signifies *Planet, satellite, comet, or astroid ephemerides, or more generally, location of any target body, given as a function of time*. Essentially, an SPK-file for any spacecraft trajectory can be produced such that the high fidelity state data can be retrieved quickly over any discrete time interval. For this analysis, the NRHO reference trajectory produced by NASA is utilized [29].

For kernel targeting, the concept is to use the kernel to quickly generate the state transition matrix $\mathbf{\Phi}_i^f$ from the current burn time t_i along the reference trajectory to a specific targeting state epoch, t_f, at any prescribed resolution Δt interval,

$$\mathbf{\Phi}_i^f = \mathbf{\Phi}_{i+n}^f \ \ldots \ \mathbf{\Phi}_{i+1}^{i+2} \ \mathbf{\Phi}_i^{i+1} \tag{29}$$

where the state transition matrix at each interval is produced with vehicle dynamics model $\mathbf{f}$ and the nominal

states $\bar{\mathbf{x}}_i$, $\bar{\mathbf{x}}_{i+1}$, ... $\bar{\mathbf{x}}_{i+n}$ extracted from the kernel.

$$\boldsymbol{\Phi}_i^{i+1} = e^{\mathbf{F}_i \Delta t_i} \qquad \text{where } \mathbf{F}_i = \left.\frac{\partial \mathbf{f}}{\partial \mathbf{x}}\right|_{\bar{\mathbf{x}}_i}$$

$$\boldsymbol{\Phi}_{i+1}^{i+2} = e^{\mathbf{F}_{i+1} \Delta t_{i+1}} \qquad \text{where } \mathbf{F}_{i+1} = \left.\frac{\partial \mathbf{f}}{\partial \mathbf{x}}\right|_{\bar{\mathbf{x}}_{i+1}}$$

$$\boldsymbol{\Phi}_{i+n}^{f} = e^{\mathbf{F}_{i+n} \Delta t_{i+n}} \qquad \text{where } \mathbf{F}_{i+n} = \left.\frac{\partial \mathbf{f}}{\partial \mathbf{x}}\right|_{\bar{\mathbf{x}}_{i+n}}$$

Given the current navigation state estimate for vehicle's position and velocity $\hat{\mathbf{x}}_i = [\hat{\mathbf{r}}_i, \hat{\mathbf{v}}_i]$ along the NRHO reference trajectory, the predicted state $\hat{\mathbf{x}}_f = [\hat{\mathbf{r}}_f, \hat{\mathbf{v}}_f]$ at the future terminal epoch t_f is generated using the state transition matrix $\boldsymbol{\Phi}_i^f$

$$\hat{\mathbf{x}}_f = \boldsymbol{\Phi}_i^f \hat{\mathbf{x}}_i \tag{30}$$

The nominal vehicle state at the terminal epoch $\bar{\mathbf{x}}_f$ can be extracted from the kernel such that the target state deviation $\delta \mathbf{x}_f$ can be expressed in terms of the state transition matrix $\boldsymbol{\Phi}_i^f$ and the initial state error $\delta \mathbf{x}_i$

$$\delta \mathbf{x}_f = \bar{\mathbf{x}}_f - \hat{\mathbf{x}}_f = \boldsymbol{\Phi}_i^f \bar{\mathbf{x}}_i - \boldsymbol{\Phi}_i^f \hat{\mathbf{x}}_i = \boldsymbol{\Phi}_i^f \left(\bar{\mathbf{x}}_i - \hat{\mathbf{x}}_i\right) = \boldsymbol{\Phi}_i^f \delta \mathbf{x}_i \tag{31}$$

Although the states extracted from the kernel or navigation filter are typically the absolute position and velocity, the states that are actually targeted can be any function $\mathbf{g}$ of these states. For example, the target state can be the final position, velocity, or any three states such as flight path angle, velocity magnitude, altitude, or orbital elements. With a single burn, three states can be targeted $\bar{\mathbf{x}}_T$ such that,

$$\bar{\mathbf{x}}_T = \mathbf{g}(\bar{\mathbf{x}}_f) \tag{32}$$

$$\hat{\mathbf{x}}_T = \mathbf{g}(\hat{\mathbf{x}}_f) = \mathbf{g}(\bar{\mathbf{x}}_f) + \mathbf{G}\delta \mathbf{x}_f + ... \tag{33}$$

where $\mathbf{G} = \frac{\partial \mathbf{g}}{\partial \mathbf{x}}|_{\bar{\mathbf{x}}_f}$. If the states targeted are the terminal position or velocity vectors, then $\mathbf{G}$ becomes,

$$\mathbf{g}(\bar{\mathbf{x}}_f) = \bar{\mathbf{r}}_f \text{ then } \mathbf{G} = [\mathbf{I}_{3\times 3}\ \mathbf{0}_{3\times 3}]$$
$$\mathbf{g}(\bar{\mathbf{x}}_f) = \bar{\mathbf{v}}_f \text{ then } \mathbf{G} = [\mathbf{0}_{3\times 3}\ \mathbf{I}_{3\times 3}]$$

Note that a variety of targeting schemes can be evaluated quickly by altering the selected states targeted $\bar{\mathbf{x}}_T$ and merely adjusting the $\mathbf{G}$ matrix. The formulation of a targeting algorithm emerges by solving for the target state deviation, $\delta \mathbf{x}_T = \bar{\mathbf{x}}_T - \hat{\mathbf{x}}_T$ to first order using Eqns 32 and 33.

$$\delta \mathbf{x}_T = \mathbf{G}\delta \mathbf{x}_f \tag{34}$$

Then substituting the definition for $\delta \mathbf{x}_f$ derived in Eqn 31 yields an expression between the initial state dispersion $\delta \mathbf{x}_i = [\delta \mathbf{r}_i\ \delta \mathbf{v}_i]$ and the terminal target state dispersion.

$$\delta \mathbf{x}_T = \mathbf{G}\boldsymbol{\Phi}_i^f \delta \mathbf{x}_i \tag{35}$$

Allow the quantity $\mathbf{G}\boldsymbol{\Phi}_i^f = [\boldsymbol{\Phi}_r\ \boldsymbol{\Phi}_v]$ such that the deviation of the desired target state $\delta \mathbf{x}_T$ can be expressed in terms mapped components of the state transition matrix $\boldsymbol{\Phi}_r$ and $\boldsymbol{\Phi}_v$

$$\delta \mathbf{x}_T = [\boldsymbol{\Phi}_r\ \boldsymbol{\Phi}_v]\delta \mathbf{x}_i \tag{36}$$

Assume at the current time an impulsive maneuver will be executed $\Delta \mathbf{v}$ such that $\delta \mathbf{x}_i = [\delta \mathbf{r}_i,\ (\delta \mathbf{v}_i + \Delta \mathbf{v})]$. Now Eqn 36 can be expanded in terms of the current deviations in position $\delta \mathbf{r}_i$ and velocity $\delta \mathbf{v}_i$ and an impulsive burn, $\Delta \mathbf{v}$.

$$\delta \mathbf{x}_T = \boldsymbol{\Phi}_r \delta \mathbf{r}_i + \boldsymbol{\Phi}_v \left[\delta \mathbf{v}_i + \Delta \mathbf{v}\right] \tag{37}$$

The required Δv needed to hit a specific set of target states at some future epoch t_f can be derived by solving for the impulsive burn

$$\Delta \mathbf{v} = \boldsymbol{\Phi}_v^{-1} \left(\delta \mathbf{x}_T - \boldsymbol{\Phi}_r \delta \mathbf{r}_i\right) - \delta \mathbf{v}_i \tag{38}$$

This assumes the selected targeted states ensure $\mathbf{\Phi}_v^{-1}$ exists. To have the targeting algorithm expressed in terms of the current state dispersions $\delta\mathbf{x}_i = \bar{\mathbf{x}}_i - \hat{\mathbf{x}}_i$ and the final state dispersions $\delta\mathbf{x}_f = \bar{\mathbf{x}}_f - \hat{\mathbf{x}}_f$, substitute in the expression in Eqn 34 where $\delta\mathbf{x}_T = \mathbf{G}\delta\mathbf{x}_f$

$$\Delta\mathbf{v} = \mathbf{\Phi}_v^{-1}\left(\mathbf{G}\delta\mathbf{x}_f - \mathbf{\Phi}_r\delta\mathbf{r}_i\right) - \delta\mathbf{v}_i \tag{39}$$

Thruster, Venting and Attitude Modeling

All the impulsive burns have execution errors due to thruster misalignment, scale factor, bias, and noise. Table 10 lists each thruster error model component. The vehicle assumes an attitude profile such that the orientation of the vehicle does not impact the resulting disturbance accelerations due to venting. The magnitude of the venting disturbance is summarized in Table 7 and captures moderate crew activity.

OPTIMIZED NRHO ORBIT MAINTENANCE TRAJECTORY CORRECTION BURN PLACEMENT

Given the robust trajectory optimization techniques and parameters introduced previously, along with the concept of operations for an NRHO orbit maintenance scenario and the assumptions regarding the GN&C system modeling, this section derives optimized number and placement of the notional Artemis III NRHO orbit maintenance trajectory correction burns. To provide a comparison, the non-optimized results from the notional baseline scenario in Table 1 with 2 NTC, 4 NTC, and 7 NTC burns are provided using three different navigation configurations: 1) Perfect Nav, 2) DSN, and 3) OpNav. Then optimized trajectory correction burn placements are derived for each navigation configuration with 2 NTC, 4 NTC, and 7 NTC burns for three different objective functions: Problem #1) minimize the total delta-v with a final NRI position dispersion constraint, Problem #2) minimize the final NRI position dispersions subject to a total delta-v constraint, and Problem #3) minimize both total delta-v and the final NRI dispersions simultaneously. The last set of analysis results determine the optimized number of trajectory correction burns and their placement for each of the three

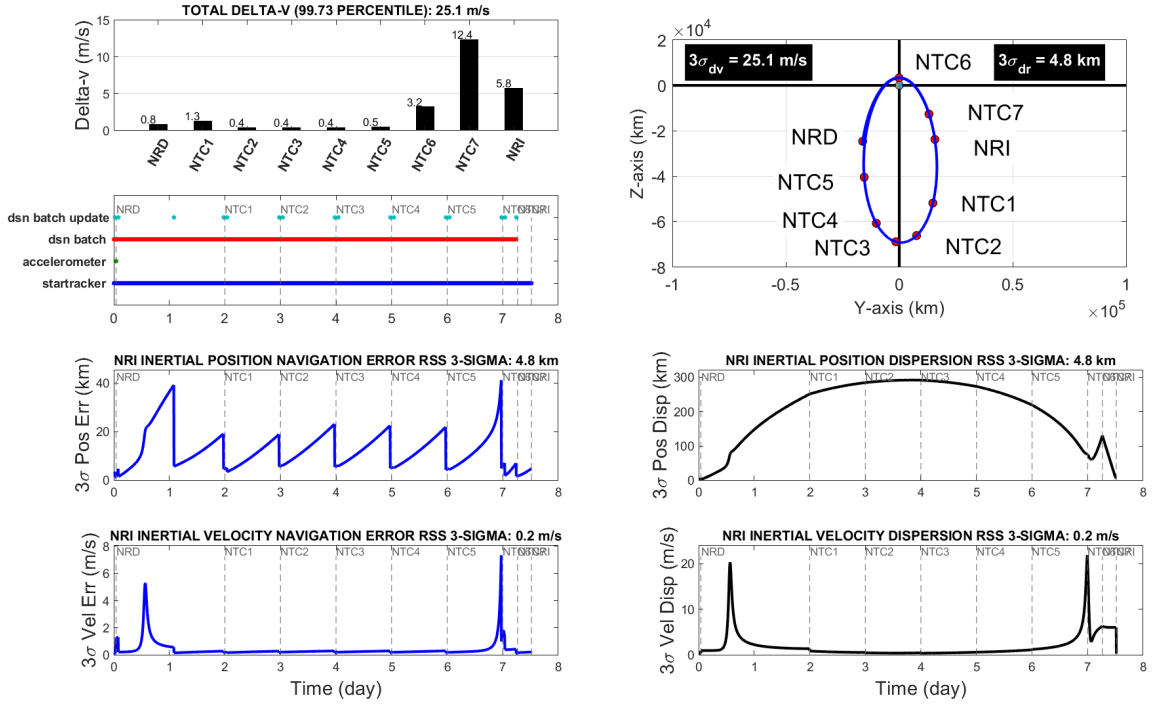

Figure 6. Performance Results with Baseline Trajectory Correction Burn Placement for 7 burns using DSN.

navigation configurations (Perfect Nav, DSN, and OpNav) and each of the three objective functions (Problem #1, Problem #2, and Problem #3).

The performance results for the baseline trajectory correction burn placement with 7 burns using DSN is provided in Figure 6. Details regarding the total delta-v are provided (top left plot) along with measurement scheduling, inertial position and velocity navigation errors, the NRHO trajectory with the simulated burn placement, and the inertial position and velocity trajectory dispersions. Rather than showing this complete data set for each optimized scenario, only the plot in the top-right quadrant is provided which includes the geometrical placement of the optimized trajectory correction burns and the resulting total delta-v ($3\sigma_{dv} = 25.1$ m/s) and the 3-sigma dispersions at NRI ($3\sigma_{dr} = 4.8$ km).

Non-Optimized Performance Results for Baseline Trajectory Correction Placement and Number

Figure 7 provides a summary of the performance for the notional baseline trajectory correction burn placement for 2 NTC, 4 NTC, and 7 NTC burns and for the different navigation configurations of perfect nav, DSN, and OpNav. The first row of plots highlight the performance using 2 NTCs. Depending on the navigation source, the total delta-v varies from 10-30 m/s with the 3-sigma NRI position dispersions ranging from 3-10 km. The second row of figures highlights the impacts of increasing the number of trajectory correction burns from 2 to 4. The last row of plots provides the performance with 7 trajectory correction burns. In this particular situation of burn placements, adding more burns does not always improve performance, particularly if they are placed near perilune or the point of closest approach to the moon. The question to answer is can both the total delta-v and the NRI trajectory dispersions be improved by optimizing the placement of each burn? If so, what level of improvement can be achieved?

Optimized Trajectory Correction Burn Placement for Ideal Navigation System (Perfect Navigation)

Figure 8 summarizes the optimized trajectory burn placement and performance when perfect navigation is assumed for situations when 2 NTC, 4 NTC, and 7 NTC burns are performed and utilizing the three different objective functions; Problem #1, Problem #2, and Problem #3. These results highlight the optimized placement due primarily to the geometry and orbital dynamics of the problem, and eliminates the impacts of the navigation system. The total delta-v can be reduced by a factor of 2-4 by optimizing the burn placement. In addition, the NRI trajectory dispersions can be reduced by a factor of 10. Trends regarding the optimized placement of the NTC burns typically has the last NTC burn (NTC7) near perilune (slightly before or after) to reduce total delta-v. To minimize position trajectory dispersions at NRI, the optimized solution places the last NTC burn (NTC7) close to NRI. One last observation is that using only 4 NTC burns instead of 7 NTCs can produce roughly the same performance when using perfect navigation.

Optimized Correction Burn Placement for Baseline Navigation System (DSN Ground Tracking)

Figure 9 highlights the impacts of using a baseline navigation system such as DSN ground tracking. Similar trends are observed as those when using perfect navigation (delta-v minimized by having NTC7 near perilune but reduce NRI dispersions by having NTC7 near NRI), but total delta-v and NRI position dispersions have increased due to the inclusion of the navigation error. Compared to using perfect nav, the total delta-v and NRI trajectory dispersions nearly double with DSN ground tracking. However, compared to the baseline burn placement, improvements by factors of 4 are observed, particularly when 7 NTC burns are incorporated in an optimized fashion. It is also noted that by shifting NTC3 from apolune (as assumed in the baseline) to 12-24 hours following the passing of the furthest distance from the moon, improvements are made (particularly for the 2-burn scenario).

Optimized Trajectory Correction Burn Placement for Backup Navigation System (OpNav)

Figure 10 shows results for a notional backup navigation system that utilizes OpNav measurements. By incorporating optimized burn placements, the total delta-v can be reduced from the baseline 30 m/s to 20 m/s for the 2-burn scenario while dropping the total delta-v from 25 m/s to less than 10 m/s for the 7-burn scenario while achieving the same NRI trajectory dispersion level near 10 km (3-sigma).

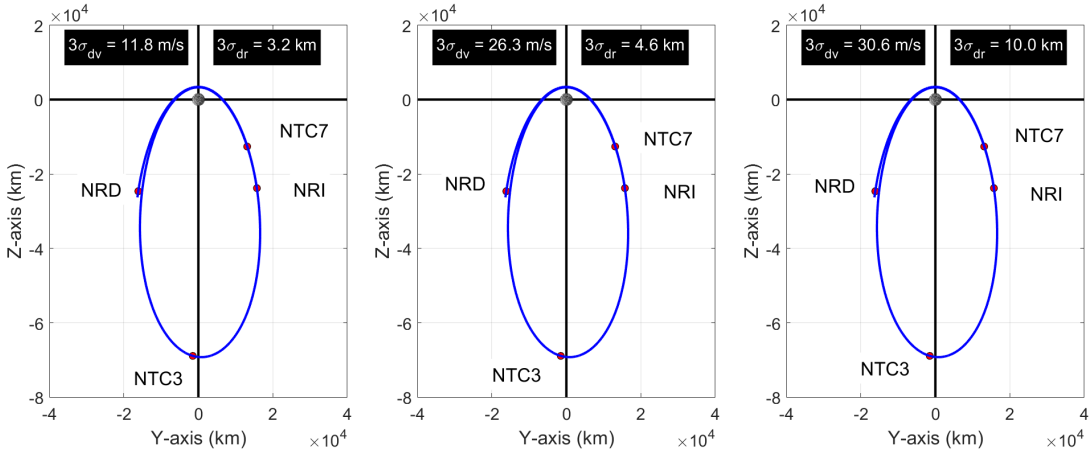

(a) 2 NTC, PERFECT NAV

(b) 2 NTC, DSN

(c) 2 NTC, OPNAV

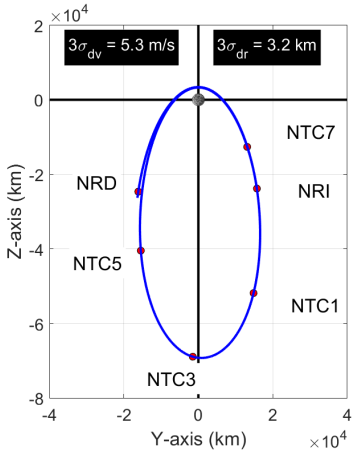

(d) 4 NTC, PERFECT NAV

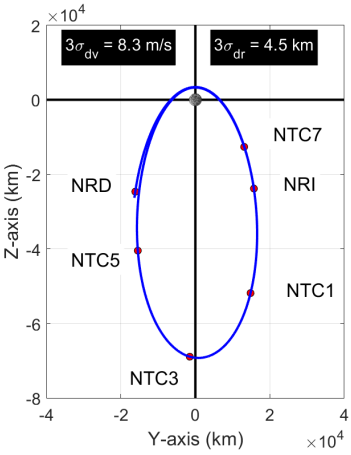

(e) 4 NTC, DSN

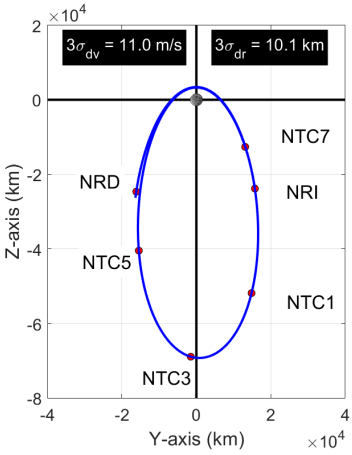

(f) 4 NTC, OPNAV

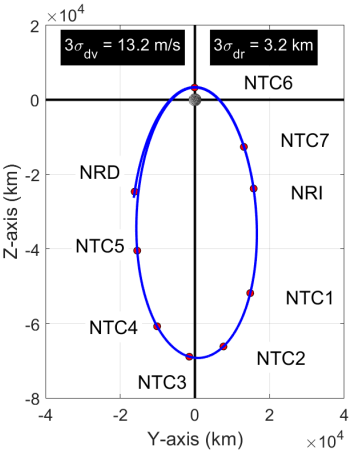

(g) 7 NTC, PERFECT NAV

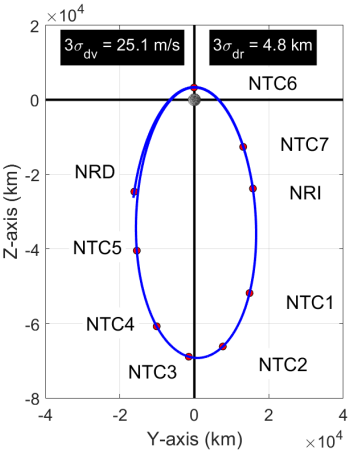

(h) 7 NTC, DSN

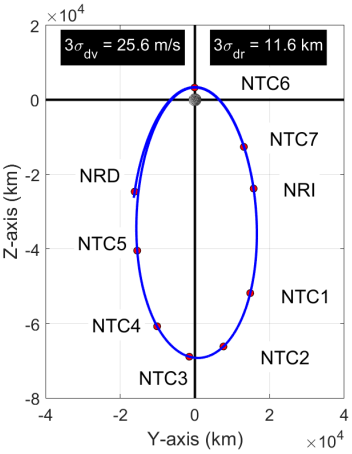

(i) 7 NTC, OPNAV

Figure 7. Non-Optimized Trajectory Burn Placement and Performance

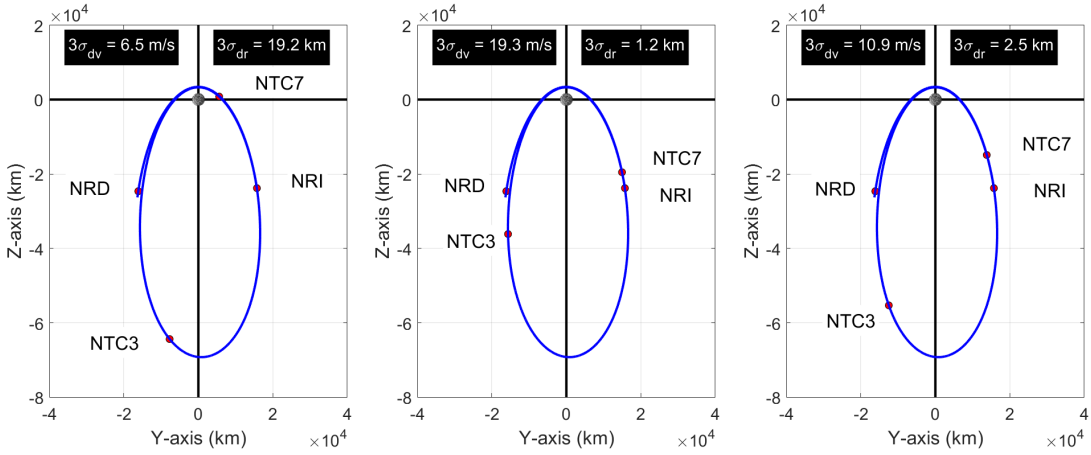

(a) 2 NTC, P1: Min DV (b) 2 NTC, P2: Min Pos Disp (c) 2 NTC, P3: Min DV and Pos Disp

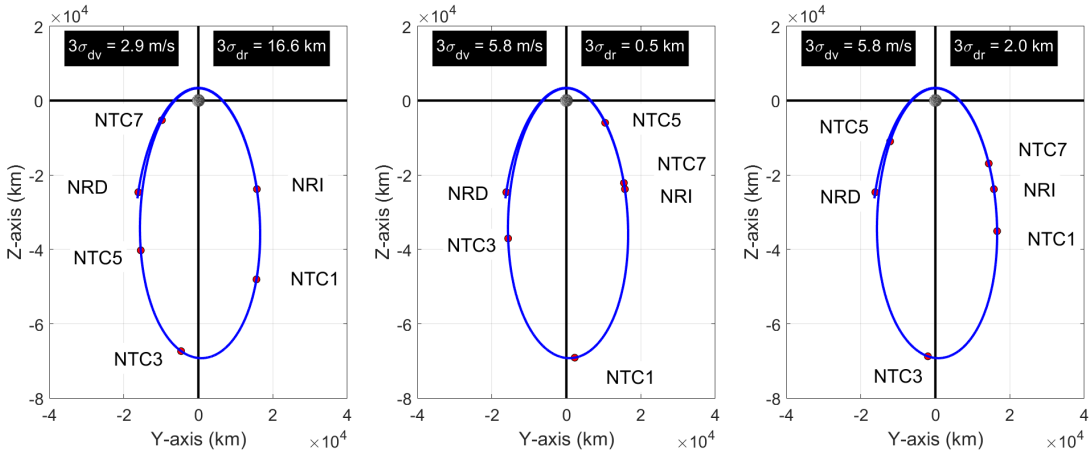

(d) 4 NTC, P1: Min DV (e) 4 NTC, P2: Min Pos Disp (f) 4 NTC, P3: Min DV and Pos Disp

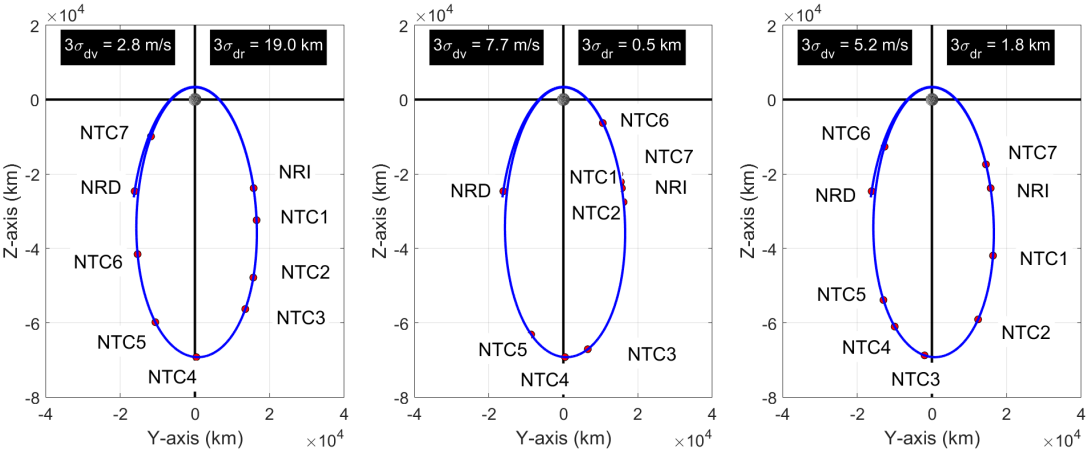

(g) 7 NTC, P1: Min DV (h) 7 NTC, P2: Min Pos Disp (i) 7 NTC, P3: Min DV and Pos Disp

Figure 8. Optimized Trajectory Burn Placement Using Perfect Navigation

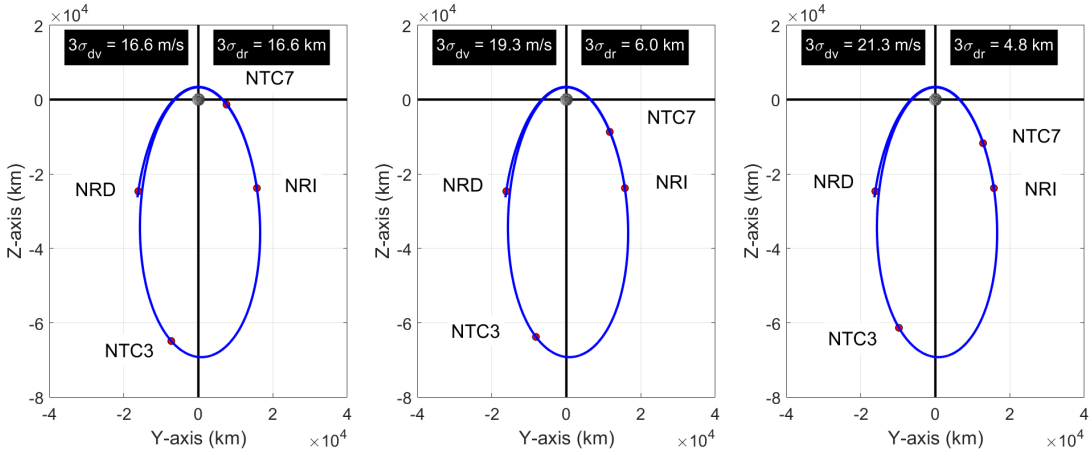

(a) 2 NTC, P1: Min DV (b) 2 NTC, P2: Min Pos Disp (c) 2 NTC, P3: Min DV and Pos Disp

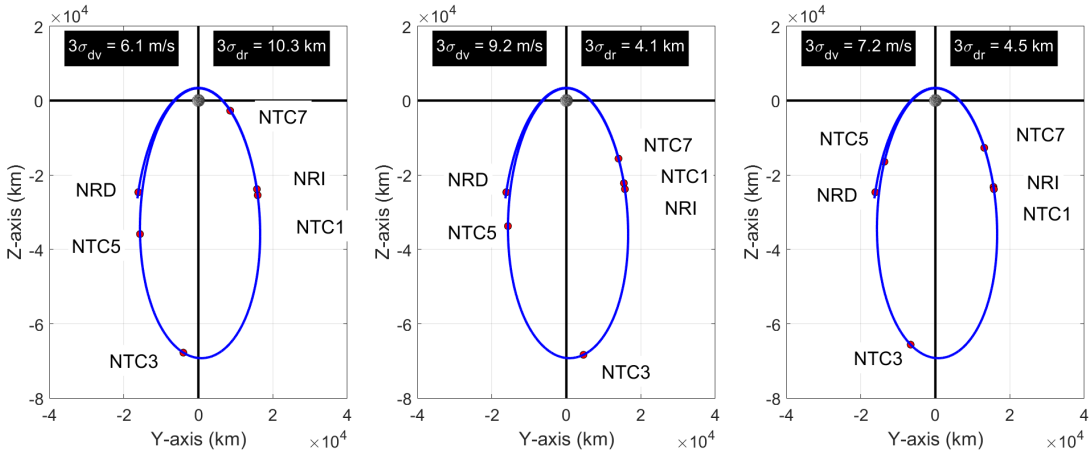

(d) 4 NTC, P1: Min DV (e) 4 NTC, P2: Min Pos Disp (f) 4 NTC, P3: Min DV and Pos Disp

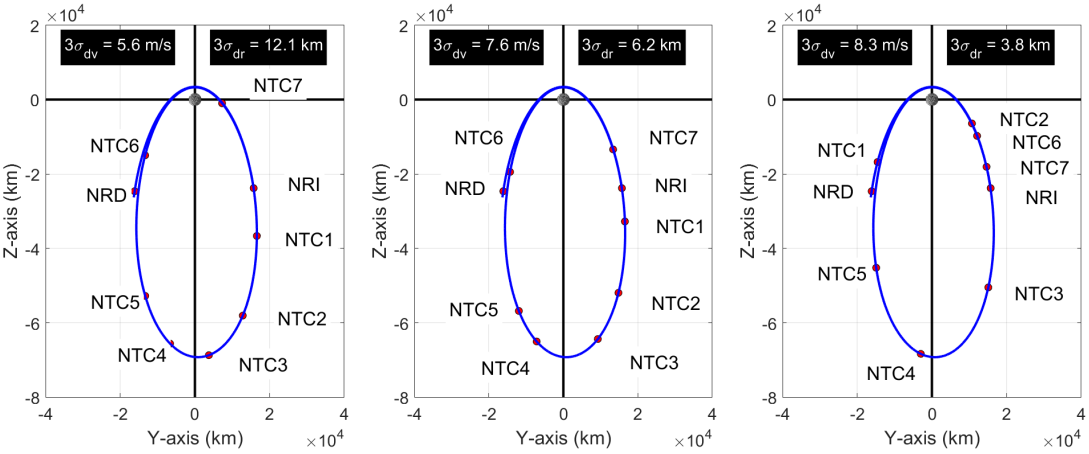

(g) 7 NTC, P1: Min DV (h) 7 NTC, P2: Min Pos Disp (i) 7 NTC, P3: Min DV and Pos Disp

Figure 9. Optimized Trajectory Burn Placement Using DSN Ground Tracking

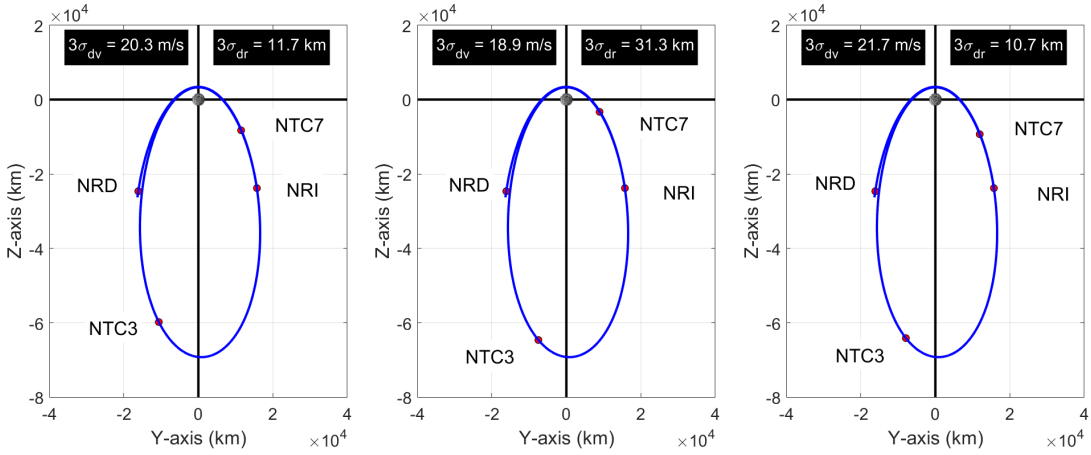

(a) 2 NTC, P1: Min DV (b) 2 NTC, P2: Min Pos Disp (c) 2 NTC, P3: Min DV and Pos Disp

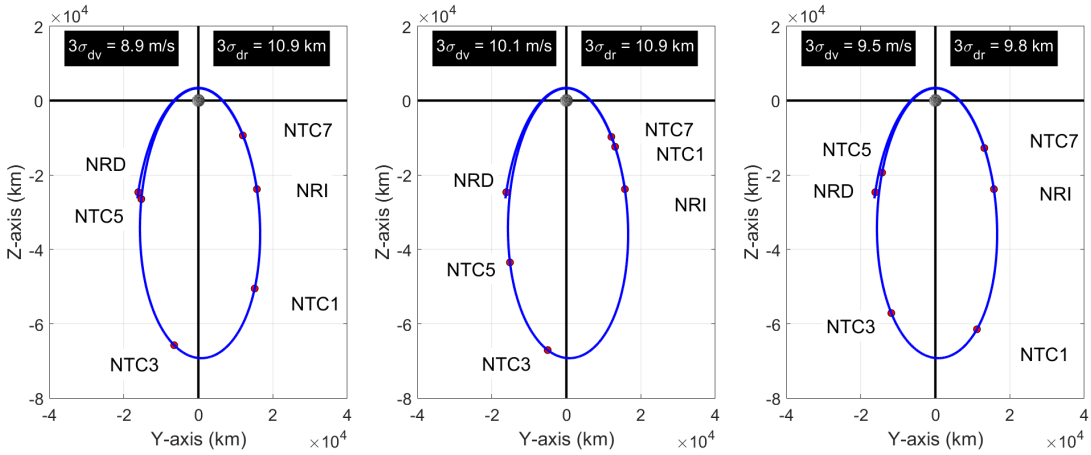

(d) 4 NTC, P1: Min DV (e) 4 NTC, P2: Min Pos Disp (f) 4 NTC, P3: Min DV and Pos Disp

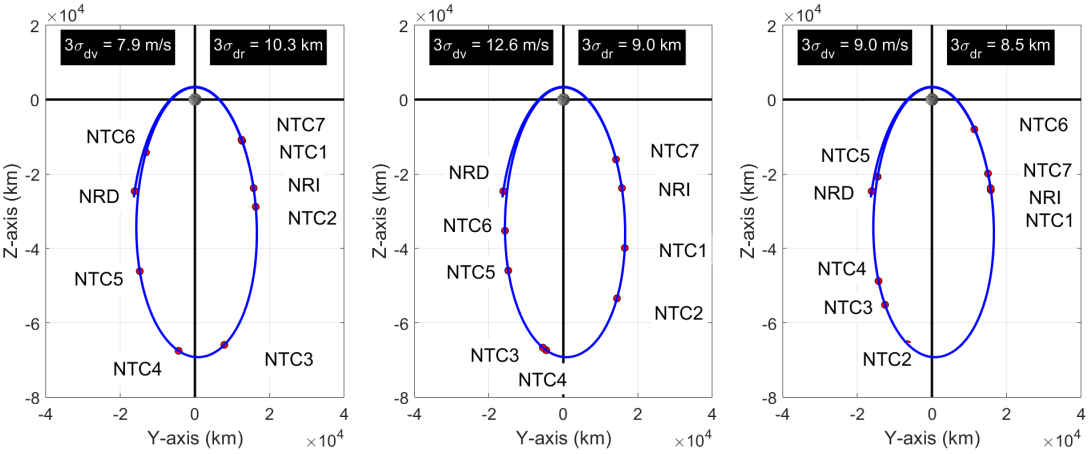

(g) 7 NTC, P1: Min DV (h) 7 NTC, P2: Min Pos Disp (i) 7 NTC, P3: Min DV and Pos Disp

Figure 10. Optimized Trajectory Burn Placement Using OpNav

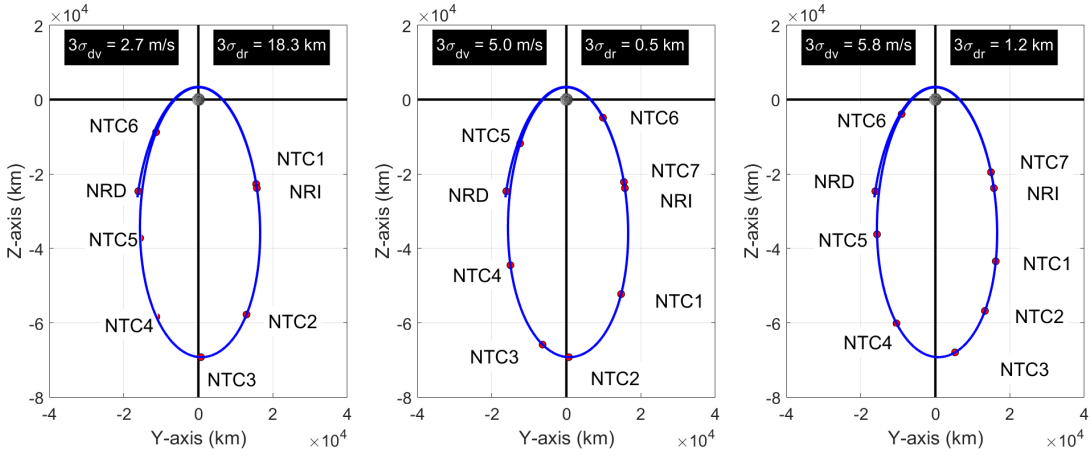

(a) PERFECT NAV, P1 (6 BURNS) (b) PERFECT NAV, P2 (7 BURNS) (c) PERFECT NAV, P3 (7 BURNS)

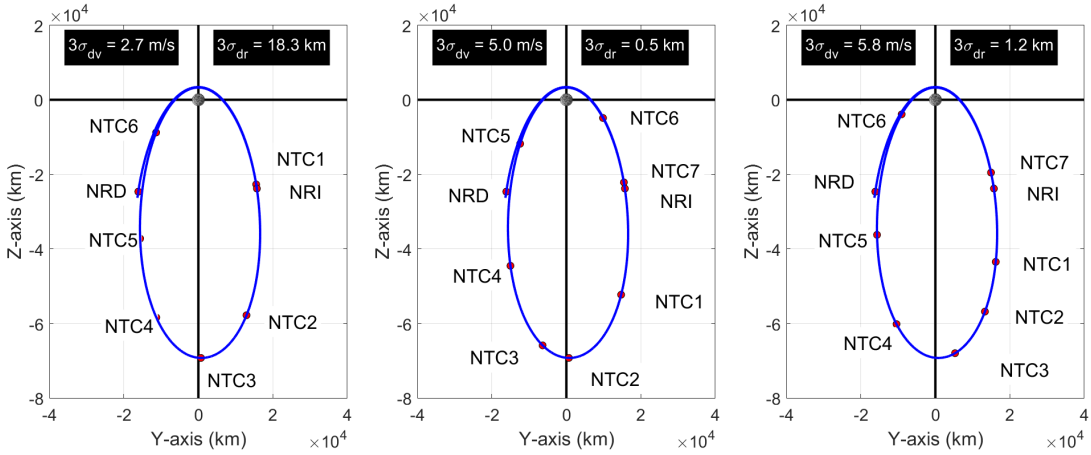

(d) DSN, P1 (UPDATE) (e) DSN, P2 (UPDATE) (f) DSN, P3 (UPDATE)

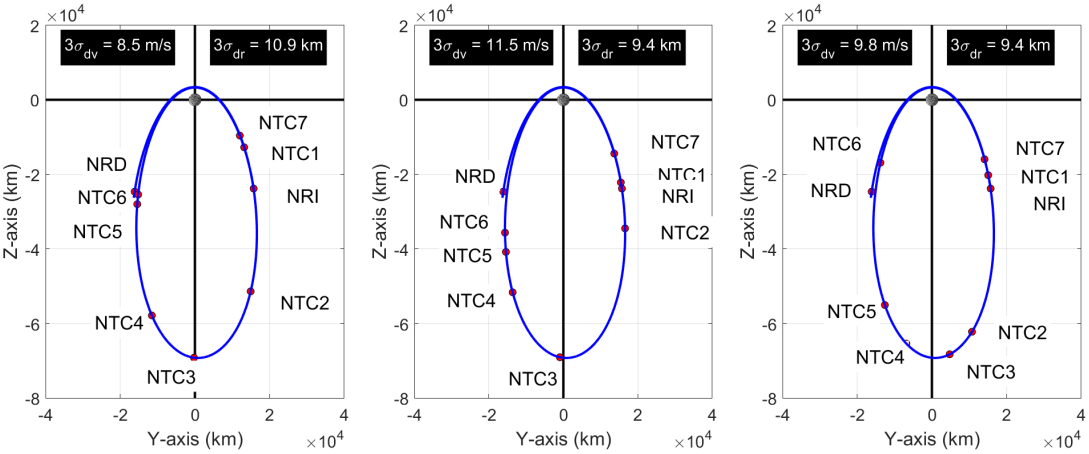

(g) OPNAV, P1 (7 BURNS) (h) OPNAV, P2 (7 BURNS) (i) OPNAV, P3 (7 BURNS)

Figure 11. Optimized Number and Placement of Trajectory Burns

Optimized Trajectory Correction Burn Placement for Reduce Number of Burns

Figure 11 investigates the optimized number of burns, not just the optimized placement of the NTC burns. Thus far a fixed set of 2 NTC, 4 NTC, and 7 NTC burns had been evaluated. For each burn, there is an operational cost and risk associated with it. If a penalty is included for each burn to account for this inherent burden to the program, then what is the optimized number of burns for cases with perfect nav, DSN, and OpNav are used and for the different objective functions Problem #1, Problem #2, and Problem #3? When using OpNav, utilizing the maximum number of burns of 7 NTC is optimal. However, for cases with perfect nav, when trying to minimize total delta-v, it is best to only perform 6 NTC burns.

CONCLUSION

With NASA's lunar exploration goals revolving around the utilization of an Earth-Moon Near Rectilinear Halo Orbit (NRHO) to facilitate access to the lunar surface while providing the long term presence of a Gateway vehicle as a staging point for both robotic and crewed missions, there emerges a growing interest to understand strategies to maintain a vehicle in an NRHO for both long durations (months and years) to shorter ones (days and weeks). For upcoming Artemis missions, the concept of NRHO orbit maintenance has a slightly different perspective than the traditional long duration focus. Rather than ensuring a spacecraft remains in an arbitrary NRHO orbit, there is a need to have a vehicle follow closely to a specific and prescribed NRHO orbit in preparation for rendezvous and docking. Current NRHO orbit maintenance strategies aim to minimize delta-v over long duration periods by allowing large phasing dispersions with the benefit of requiring few orbit maintenance burns. To support RPOD operations where the trajectory control of one vehicle impacts the performance of another, NRHO orbit maintenance now has an altered purpose where the phasing must be controlled at the likely expense of increased propellant usage.

As a result, this work attempts to provide preliminary performance results that identify optimized trajectory correction burn placement using non-traditional robust trajectory optimization techniques for short term NRHO orbit maintenance. By combining linear covariance analysis and a genetic algorithm, uncertainty in the system can be accommodated and trajectory correction burns which are nominally zero, can be strategically placed to reduce total delta-v (nominal + 3-sigma dispersions) while ensuring the vehicle remains close to a specific NRHO reference trajectory. Arbitrarily selecting the number and placement of the NRHO trajectory correction burns can lead to an increase of delta-v by a factor of 5 when including uncertainties in the design process. The sensitivity to burn placement as a function of the navigation system and the selected optimization objective functions is also provided. Attempts are also made to start identifying the optimized number of burns required to help reduce the operational costs and risks, while still achieving performance requirements.

REFERENCES

[1] J. Williams, D. E. Lee, R. J. Whitley, K. A. Bokelmann, D. C. Davis, and C. F. Berry, "Targeting Cislunar Near Rectilinear Halo Orbits for Human Space Exploration," *American Astronautical Society*, 1017, pp. AAS 17–267.

[2] D. J. Grebow, M. T. Ozimek, K. C. Howell, and D. C. Folta, "Multibody Orbit Architectures for Lunar South Pole Coverage," *Journal of Spacecraft and Rockets*, Vol. 45, No. 2, March-April 2008.

[3] D. Guzzetti, E. Zimovan, K. Howell, and D. Davis, "Stationkeeping Analysis for Spacecraft in Lunar Near Rectilinear Halo Orbits," *27th AAS/AIAA Space Flight Mechanics Meeting*, San Antonio, TX, AAS 17-395, February 2017.

[4] D. Davis, S. Bhatt, K. Howell, J.-W. Jang, R. Whitely, F. Clark, D. Guzzetti, E. Zimovan, and G. Barton, "Orbit Maintenance and Navigation of Human Spacecraft at Cislunar Near Rectilinear Halo Orbits," *27th AAS/AIAA Space Flight Mechanics Meeting*, San Antonio, TX, AAS 17-269, February 2017.

[5] P. S. Maybeck, *Stochastic models, estimation, and control*, Vol. 1. New York: Academic Press, 1979.

[6] D. K. Geller, "Linear Covariance Techniques for Orbital Rendezvous Analysis and Autonomous Onboard Mission Planning," *Journal of Guidance, Control, and Dynamics*, Vol. 29, November-December 2006, pp. 1404–1414.

[7] K. Jin, D. K. Geller, and J. Luo, "Robust Trajectory Design for Rendezvous and Proximity Operations with Uncertainties," *Journal of Guidance, Control, and Dynamics*, Vol. 43, No. 4, 2020, pp. 741–753.

[8] D. K. Geller, S. Shuster, D. Woffinden, and S. Bieniawski, "Robust Cislunar Trajectory Optimization via Midcourse Correction and Optical Navigation Scheduling," *44th Annual AAS Guidance, Navigaiton and Control Conference*, Breckenridge, CO, AAS 22-065, 4-9 February 2022 2022.

[9] D. Woffinden, S. Shuster, and S. Geller, David Kand Bieniawski, "Robust Trajectory Optimization and GN&C Performance Analysis For NRHO Rendezvous," *2022 AAS/AIAA Astrodynamics Specialist Conference*, Charlotte, North Carolina, 22-564, 7-11 August 2022 2022.

[10] D. Geller, D. Woffinden, and S. Bieniawski, "Sensitivity of Optimal Midcourse Correction Scheduling for Robust Cislunar Trajectory Design," Breckenridge, CO, AAS 23-061, 1 Feb - 6 Feb 2023.

[11] T. Goulet, D. Woffinden, N. Collins, and B. Andrews, "Robust Trajectory Design for Rendezvous in a Near Rectilinear Halo Orbit," Breckenridge, CO, AAS 23-066, 1 Feb - 6 Feb 2023.

[12] G. Calkins, D. Woffinden, and Z. Putnam, "Robust Trajectory Optimization for Guided Powered Descent and Landing," *2022 AAS/AIAA Astrodynamics Specialist Conference*, Charlotte, NC, AAS 22-660, 7-11 August 2022 2022.

[13] J. Joshi, D. Woffinden, and Z. Putnam, "End-to-End Mars Aerocapture Analysis Using Linear Covariance Techniques and Robust Trajectory Optimization," *2022 AAS/AIAA Astrodynamics Specialist Conference*, Charlotte, NC, AAS 22-678, 7-11 August 2022 2022.

[14] D. Woffinden, R. Eckman, and S. Robinson, "Optimized Trajectory Correction Burn Placement for the NASA Artemis II Mission," Breckenridge, CO, AAS 23-062, 1 Feb - 6 Feb 2023.

[15] T. J. Moesser and D. K. Geller, "Guidance and Navigation Linear Covariance Analysis for Lunar Powered Descent," *AAS/AIAA Astrodynamics Specialist Conference*, Mackinac Island, Michigan, AAS 07-313, 19-23 August 2007.

[16] D. Geller and D. Christensen, "Linear Covariance Analysis for Powered Lunar Descent and Landing," *The Journal of Spacecraft and Rockets*, Vol. 46, Nov-Dec 2009, pp. 1231–1248.

[17] D. Woffinden, S. Robinson, J. Williams, and Z. Putnam, "Linear Covariance Analysis Techniques to Generate Navigation and Sensor Requirements for the Safe and Precise Landing - Integrated Capabilities Evolution (SPLICE) Project," *AIAA Scitech 2019 Forum*, San Diego, CA, AIAA 2019-0662, 7-11 January 2019 2019.

[18] J. W. Williams, W. E. Brandenburg, D. C. Woffinden, and Z. R. Putnam, "Validation of Linear Covariance Techniques for Mars Entry, Descent, and Landing Guidance and Navigaiton Performance Analysis," *AIAA Scitech 2022 Forum*, 2022, 10.2514/6.2020-0597.

[19] D. Woffinden, S. Bhatt, D. Kirkpatrick, and P. Spanos, "Optimal Multi-Variable Multi-Constraint Spacecraft GN&C Requirement Derivation," *41st Annual AAS Guidance and Control Conference*, Breckenridge, CO, AAS 18-095, 5-10 Feb 2018.

[20] M. Mitchell, *An Introduction to Genetic Algorithms*. 1996.

[21] B. C. Collicott and D. C. Woffinden, *Lunar Navigation Performance using the Deep Space Network and Terrain Relative Navigation to Support Precision Landing*. 19-21 January 2021, 10.2514/6.2021-0375.

[22] G. N. Holt, C. N. D'Souza, and D. Saley, "Orion Optical Navigation Progress Toward Exploration Mission 1," *AIAA Scitech 2018 Forum, Space Flight Mechanics Meeting*, Kissimmee, Florida, AIAA 2018-1978, 8-12 January 2018 2018.

[23] A. M. Dwyer-Cianciolo, C. D. Karlgaard, D. Woffinden, R. A. Lugo, J. Tynis, R. R. Sostaric, S. Striepe, R. Powell, and J. M. Carson, "Defining Navigation Requirements for Future Missions," *AIAA Scitech 2019 Forum*, San Diego, 2019. 2019-0661, 10.2514/6.2019-0661.

[24] B. G. Marchand, K. Howell, and R. Wilson, "Improved Corrections process for Constrained Trajectory Design in the n Body Problem," *Journal of Spacecraft and Rockets*, Vol. 35, July 2007, pp. 1–33, 10.2514/1.27205.

[25] M. W. Weeks, B. G. Marchand, C. W. smith, and S. Scarritt, "Design of the Onboard Autonomous Targeting Algorithm for the Trans-Earth Phase of Orion," Honolulu, Hawaii, AIAA Guidance, Navigation and Control Conference and Exhibit, 18-21 August 2008.

[26] B. G. Marchand, M. W. Weeks, C. W. Smith, and S. Scarritt, "Onboard Autonoous Targeting for the Trans-Earth Phase of Orion," *Journal of Guidance, Control, and Dynamics*, Vol. 33, May-June 2010, pp. 943–956, 10.2514/1.42384.

[27] S. Scarritt, B. G. Marchand, A. J. Brown, W. H. Tracy, and M. W. Weeks, "Finite-Burn Linear Targeting Algorithm for Autonomous Path Planning Guidance," *Journal of Guidance, Control, and Dynamics*, Vol. 35, September-October 2012, pp. 1605–1615, 10.2514/1.54249.

[28] S. K. Scarritt, T. Fill, and S. Robinson, "Advances in Orion's On-Orbit Guidance and Targeting System Architecture," Breckenridge, CO, AAS 15-096, 1 Feb - 6 Feb 2015.

[29] D. E. Lee, "White Paper: Gateway Destination Orbit Model: A Continuous 15 year NRHO Reference Trajectory"," *Tech Report. Document ID: 20190030294,*, NASA Johnson Space Center, Houston, TX, National Aeronautics and Space Administration, 20 August 2019 2019.